Technological Developments and Future Perspectives in Particle Therapy: A Topical Review

Aafke Christine Kraan and Alberto Del Guerra

***Abstract*—In the last decades, important technological progress has been made to enhance the quality and efficiency of particle therapy treatments. Continuous improvements in dose delivery, treatment planning and verification techniques have led to higher-dose conformity and better sparing of healthy tissue. At the same time, particle therapy treatments are complex and much more expensive than conventional radiotherapy, and only highly specialized facilities can offer these treatments. Cost reduction is thus a strong drive behind technological developments in the field. The number of treatment facilities offering proton and carbon therapy has strongly grown in the last decades, and the amount of research efforts and innovations have increased continuously. From a technological perspective, advances in hardware are often accompanied by innovations in software and computation, and vice versa. In this review we will present a basic overview of technological advances in particle therapy hardware (accelerators, gantries, applications of superconductivity, treatment verification techniques), software (Monte Carlo simulations, treatment planning calculations), and studies toward clinical applications. By combining a broad selection of topics into a single review and by covering both proton and carbon therapy, we aim at providing the reader a unique overview of the evolution of various technologies developed for particle therapy.**

***Index Terms*—Accelerators, Monte Carlo simulations, particle therapy, review, technological developments, treatment planning, treatment verification.**

I. Introduction

PARTICLE therapy is an external beam radiotherapy where the dose is delivered using beams of light ions, defined here as nuclei with an atomic number lower or equal to 10, i.e., ions from protons to neon. Over the past decades, technological advances have transformed particle therapy from a research topic into a powerful and precise treatment modality for cancer patients. Technological innovations in this field have been mainly driven by the necessity of increasing treatment efficacy. Improvements in tumor localization and dose delivery have resulted in high-quality treatments, characterized by high-dose conformity and excellent sparing of organs at risk. Today particle therapy represents an important therapeutic component in the multidisciplinary management of various types of cancer, including pediatric, head-and-neck, brain, prostate, breast, and gastrointestinal cancer patients [1], [2]. Fig. 1 shows the result of a patient that was affected by sinonasal teratocarcinosarcoma and treated at the National Center for Oncological Hadrontherapy (CNAO) in Pavia, Italy, with the computed tomography (CT) scan before [Fig. 1(a)] and 10 months after treatment with proton therapy and radiosensibilizing chemotherapy [Fig. 1(b)]. The proton therapy treatment plan is shown in Fig. 1(c). Tumor regression can be clearly observed in the affected region (yellow square), while radiation toxicity was minimal.

Despite its high potential, most hospitals in the world do not offer particle therapy treatments yet. A major obstacle is the high cost associated with a particle therapy treatment with respect to a conventional radiotherapy treatment. Although vendors are offering more and more cost-competitive solutions today, there is still a large gap in costs between a photon and a particle therapy treatment. This is primarily caused by the installation and operational costs, requiring expensive equipment and high-expertise and trained personnel. A second obstacle is the large size of a typical particle therapy machine, due to the accelerator and gantry. In the last years, commercial companies offer compact solutions for beam acceleration and delivery, but the excessive size remains a major issue today, in particular for carbon therapy. Reducing the treatment costs and the dimensions of particle therapy installations is therefore a strong drive for technological innovations.

Various recent detailed reviews about particle therapy hardware technologies are available [3], [4], [5], [6], as well as overviews of radiobiological advances [7], [8], [9], Monte Carlo (MC) simulations [10], [11], treatment planning [12], [13], treatment verification techniques [14], and applications of artificial intelligence (AI) in particle therapy [15]. Future directions in proton and particle therapy are discussed by Mohan [16] and Graeff et al. [17], respectively. We decided to adopt a broader approach, by covering all these topics within a single topical review, where we present

Manuscript received 15 June 2023; revised 12 January 2024; accepted 25 February 2024. Date of publication 11 March 2024; date of current version 3 May 2024. This work was supported in part by PNRR M4.C2.1.1. under Grant PRIN2022CWXR8K—CUP 153D23000520006. *(Corresponding author: Aafke Christine Kraan.)*

This work includes figures that involved human subjects in its research, where some (Figs. 20 and 22) were taken from other publications, in which was stated that they were approved by the local ethics committee. Regarding Fig. 10, the authors confirm that the human subject research procedures and protocols are exempt from review board approval. Figs. 1 and 16 are original figures, reviewed and approved by the Comitato etico del Policlinico San Matteo di Pavia, Italy, and the patients/participants provided their written informed consent to participate in this study. None of the figures in this work includes information that could lead to identification of the patients/participants.

Aafke Christine Kraan is with Istituto Nazionale di Fisica Nucleare, Sezione di Pisa, 56127 Pisa, Italy (e-mail: aafke.kraan@pi.infn.it).

Alberto Del Guerra is with the Department of Physics, University of Pisa, 56126 Pisa, Italy.

Color versions of one or more figures in this article are available at https://doi.org/10.1109/TRPMS.2024.3372189.

Digital Object Identifier 10.1109/TRPMS.2024.3372189

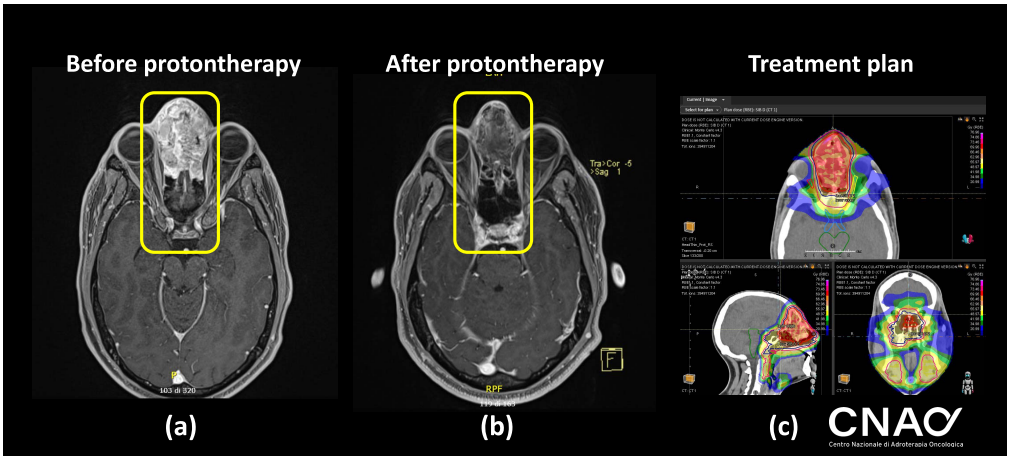

Fig. 1. Treatment findings of a patient affected by sinonasal teratocarcinosarcoma treated at CNAO, with a CT slice before (a) and 10 months after (b) treatment with radiosensibilizing chemotherapy and proton therapy. The delivered proton therapy treatment plan is shown in (c), where the red zone corresponds to 70 Gy (RBE) delivered in 33 fractions. Tumor regression can be clearly observed in the tumor region (yellow square). Figure courtesy of V. Vitolo (CNAO).

past, present and future of technological developments in particle therapy. The rationale was that most of these topics are interconnected. For some aspects we only present the basic concepts that are necessary to comprehend particle therapy technology and refer to the cited references for a more complete description [3], [4], [5], [6], [7], [8], [9], [10], [11], [12], [13], [14].

Advances in hardware are often seen to be accompanied by innovations in software and computation techniques, and vice versa. As an example, the pencil beam scanning (PBS) technology has lead to new treatment planning calculation and optimization strategies. And vice-versa, MC simulations have played an essential role in the design and realization of hardware, such as shielding devices and experimental setups for treatment verification. In this review we will therefore discuss progress in a variety of hardware and software topics, as well as their clinical applications. More specifically, we review ongoing progress in: accelerators, beam delivery and transport systems, including superconductive solutions, MC simulations, treatment plan calculations, radiobiology, and treatment verification strategies. The emphasis of this work will be on technologies that are clinically or experimentally applied or close to a clinical application, but some future technologies will also be discussed. We include advantages, disadvantages, challenges, limitations and, where relevant, comparisons. For those who are new to the field this review could serve as a concise introduction to the various technologies available in particle therapy; for those already involved it could be a useful guide to extra literature with more technical details and references. As a final remark, we remind that the selection of technologies and literature that will be highlighted in this article should be considered as nonexhaustive.

II. Accelerators

Technological developments in accelerators for particle therapy are driven by clinical efficiency and cost considerations. In this section we summarize the most commonly used accelerators, as well as a few emerging technologies. For more extensive reviews about accelerators in particle therapy we refer to dedicated works and references therein [3], [4], [6], [18], [19].

A. Cyclotrons

The first particle therapy patient treatments by Lawrence in the 1950's were done with protons from a 60 inch cyclotron in Berkeley (USA) [20], using a 220 tons magnet. The first hospital-based proton therapy center for ocular melanomas was opened in 1989 at the Clatterbridge Cancer Centre (U.K.), using a 60-MeV cyclotron. It was only in 1998 that the first dedicated commercial proton-therapy cyclotron was clinically used, at National Cancer Center in Kashiwa (Japan) [21], followed three years later by the Massachusetts General Hospital [22].

In a cyclotron, particles are extracted from a source positioned at the center of the cyclotron. A radio-frequency (RF) system provides a strong electric field, accelerating the particles between electrode plates through repetitive crossing. The particles are confined into a spiral-shaped orbit by a high-field magnet. Once the particles have reached their maximum energies (typically 230–250 MeV for protons), an extraction system guides the particles out of the cyclotron into a beam-transport system. A beam degrader system is needed to obtain the desired particle energy. This is typically an absorber of variable thickness (see Section III-B), leading to the production of secondaries and stray radiation. Various types of cyclotrons have been developed over the last decades.

Classical cyclotrons are based on resistive coils and fixed-field electromagnets. They are operated at a fixed RF and all the settings of the beam lines are fixed, making them relatively easy to operate. The first patient treatments by Lawrence were done with a classical cyclotron. During acceleration, the relativistic mass increases with increasing energy. The particles gradually run out of phase with respect to the RF system, and deceleration steps in at some point.

In isochronous cyclotrons the magnetic field increases with the radial distance from the center toward the extraction radius, while the RF frequency is fixed. This allows to

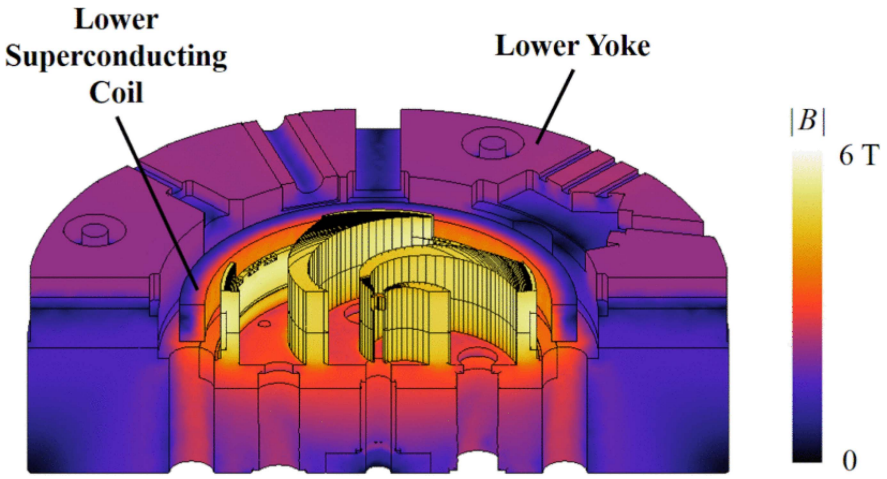

Fig. 2. Magnetic field distribution in the superconducting isochronous cyclotron at the magnet excitation test phase. Reproduced from [24].

compensate for relativistic effects, and higher energies can be reached. Most early patient treatments were done with isochronous cyclotrons [21]. At present, they are still the most widely applied accelerators for proton therapy, and have been produced and installed by large vendors, such as Proteus 235 and C230 by Ion Beam Applications (IBA, Louvain-La-Neuve, Belgium).

The large weight (100–200 tons) and size (typically 3–4-m diameter) associated with conventional magnets pose technical challenges to the installation of these systems in a hospital environment. The application of superconducting magnets allows for a large size and weight reduction, because strong magnetic fields can be generated while keeping the size of coils relatively small. The first superconducting isochronous cyclotron for proton therapy was installed at the Paul Scherrer Institute (PSI) [23] in Villigen, Switzerland. This type of cyclotron is today adopted in several commercial proton therapy systems, such as ProBeam system (Varian, Palo Alto, CA, USA) and the ProNova SC360 system (Pronova Solutions, Maryville, TN, USA). Conceptual designs of other compact superconducting isochronous cyclotrons for proton therapy are available, including a compact and lighter weight (65 tons) version by Sumitomo Heavy Industries Ltd (Ehime, Japan) [24], which is shown in Fig. 2. This manufacturer has also performed design studies for superconducting isochronous cyclotrons for carbon therapy [25]. An isochronous superconducing cyclotron is also chosen in the C400 Archade accelerator prototype, currently being developed for carbon and helium therapy by IBA and NHa (Normandy Hadrontherapy Caen, France) [26] In Dubna (Russia) feasibility studies are ongoing to develop a compact accelerator for carbon therapy, based on a dual isochronous cyclotron design [27]. The current challenges for the acceleration of carbon ions with superconducting cyclotrons include the mechanical stability, deformations, large weight of the return yoke, resonances, design of compact cooling systems, stability of the beam current, and cost effectiveness [25], [26], [27], [28].

An alternative accelerator type is the synchrocyclotron. Here, the magnet strength is constant with radial distance, but the frequency of the RF electric field is decreased in synchronism with the increasing velocity of the particle to compensate for relativistic effects. This cyclotron type was used for many patient treatments at Harvard University for several decades [29]. Advances in magnet technology have led to the development of superconducting synchrocyclotrons, allowing for a reduction in size, magnet weight and cost. Today, many single room proton therapy installations are based on this technology. An example is the S250 system (Mevion, Littleton, MA, USA), where a 20 tons superconducting synchrocyclotron has been mounted on a gantry rotating around the patient [30]. This system applies the scatter technique (see Section III-A), with range modulators for energy variations and multileaf collimators for shaping the beam. Another single-room system is the 20 tons superconducting S2C2 synchrocyclotron, used in the Proteus-One system (IBA, Louvain-La-Neuve, Belgium) [31]. In this case proton beams are delivered with spot scanning. At present, about 40 single-room systems are installed or planned worldwide, compared to about a hundred total active proton therapy facilities [21]. The amount of single-room installations will continue to grow.

Although the presently installed superconducting synchrocyclotrons are much lighter than normal conducting cyclotrons, even lighter systems are desired. Much research today is focused on the development of iron-free synchrocyclotrons. In such devices superconducting coils are not only used as magnet poles, but also as return yoke and magnetic shielding [28]. Such ultralight systems can easily be mounted directly on a gantry, eliminating beam-transport magnets.

B. Synchrotrons

A synchrotron was used for the heavy ion therapy pilot project, that started in 1975 at the Lawrence Berkeley Laboratory (LBL). It used He, C, Ne, Si, and Ar ions [32]. The first hospital-based proton-therapy facility that could be used for a large number of treatment sites was at Loma Linda (USA), using a synchrotron accelerator with energies from 70 to 250 MeV, designed and built at Fermilab. The first patients were treated in October 1990 [33].

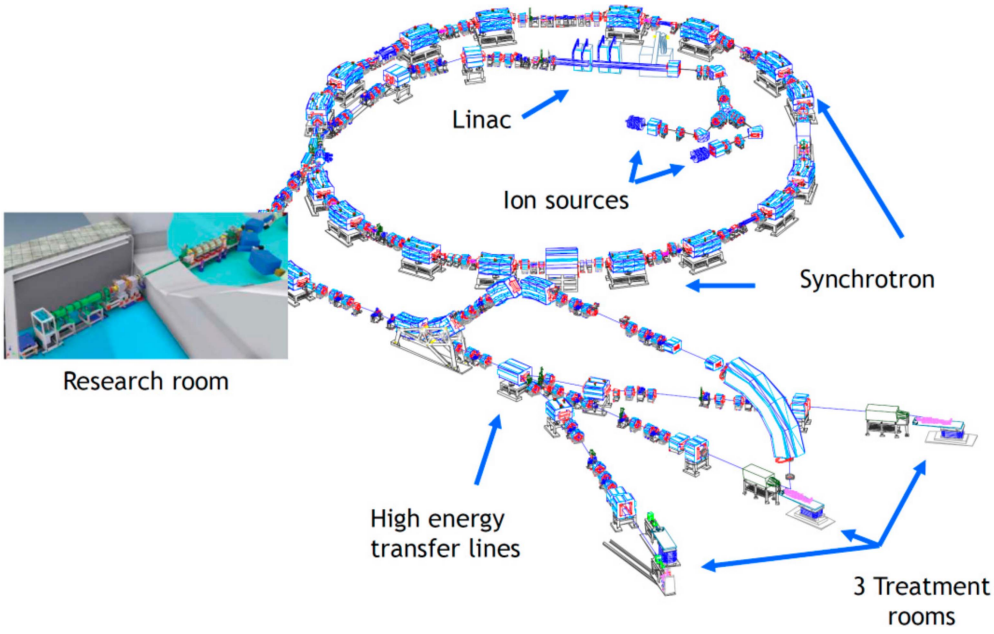

Fig. 3. Model of the CNAO synchrotron, with the injection chain located inside the ring and three horizontal beamlines and one experimental room. The diameter of the synchrotron is about 25 m. In the future a superconducting rotating gantry is foreseen. From [36], used under the creative common CC BY license.

In a synchrotron, particles are injected into a ring, consisting of an array of quadrupole and dipole magnets for focusing and bending the beam, respectively, connected by straight linear sections. In one or more of those sections RF cavities are installed to accelerate the particles. Both the magnitude of the magnetic fields and the RF frequency are varied in order to maintain synchronous particles at a constant orbit radius. Synchrotrons have a beam with a bucket structure. Since the particles can go around the accelerator ring many times, high energies can be obtained. An advantage of synchrotrons with respect to cyclotrons is that the beam energy can be easily varied, a beam degrader is not required, and the synchrotron has a low amount of stray radiation. The complexity of shielding design, maintenance during operation and decommissioning at the end of lifetime is related to the amount of activated materials. Therefore, these issues are generally considered somewhat easier for synchrotrons than for cyclotrons (see for instance a report by the International Atomic Energy Agency [34]). Another advantage of synchrotrons is the possibility of offering treatments with different ions.

Today, about one quarter of the proton therapy facilities makes use of synchrotons. Several commercial vendors of proton therapy synchrotons exist. ProTom developed a light (15 tons) and compact (5-m diameter) system called Radiance 330 that delivers beams with energies up to 250 MeV, with the possibility to upgrade up to 330 MeV. This system is installed a few locations worldwide, including Massachusetts General Hospital. Other commercial vendors of proton therapy synchrotrons include Hitachi and Mitsubishi.

For carbon therapy, the first synchroton used for patient treatments was in 1994 at the National Institute of Radiological Sciences (NIRS) in Chiba, Japan [35], currently part of the National Institute for Quantum Science (QST). Today synchrotrons are still the only solution used for carbon therapy worldwide, with a typical maximum energy of 400–430 MeV/u.

At present there are 14 carbon ion therapy centers operational in the world [21]. Only a few centers offer both protons and carbon treatments. Among these is CNAO in Italy [36], which was designed and developed thanks to the collaboration between the Proton–Ion Medical Machine Study (PIMMS) project, the TERA (therapies with hadronic radiation) foundation [37], CERN (European Organization for Nuclear Research) and INFN (National Institute for Nuclear Physics, Italy. Fig. 3 shows the layout of the accelerator and beamlines of the CNAO synchroton. Other beams than protons and carbon ions are planned in the future, as well as a rotating superconducting gantry [38].

Despite the radiobiological advantages of carbon ions over protons, the excessive size and the operational costs of synchrotrons for carbon therapy pose a substantial barrier to their widespread application. The current facilities are all based on normally conducting magnet technologies, leading to synchrotrons with a diameter of about 60 m. Efforts are ongoing in applying superconducting magnets, allowing for a reduction of the diameter of the accelerator and of the size and weight of the magnets.

The development of carbon ion technology is mostly carried out in research laboratories. At the QST-NIRS facility in Japan, intense research is ongoing to develop an extremely compact (10 m $\times$ 20 m) single room machine based on superconducting magnets and laser acceleration technologies (Quantum Scalpel) [39]. In the design of turning linac for proton therapy (TULIP) [40], a high-gradient linear accelerator is proposed to accelerate particles, which can rotate around the patient couch. Efforts are also ongoing to reduce the

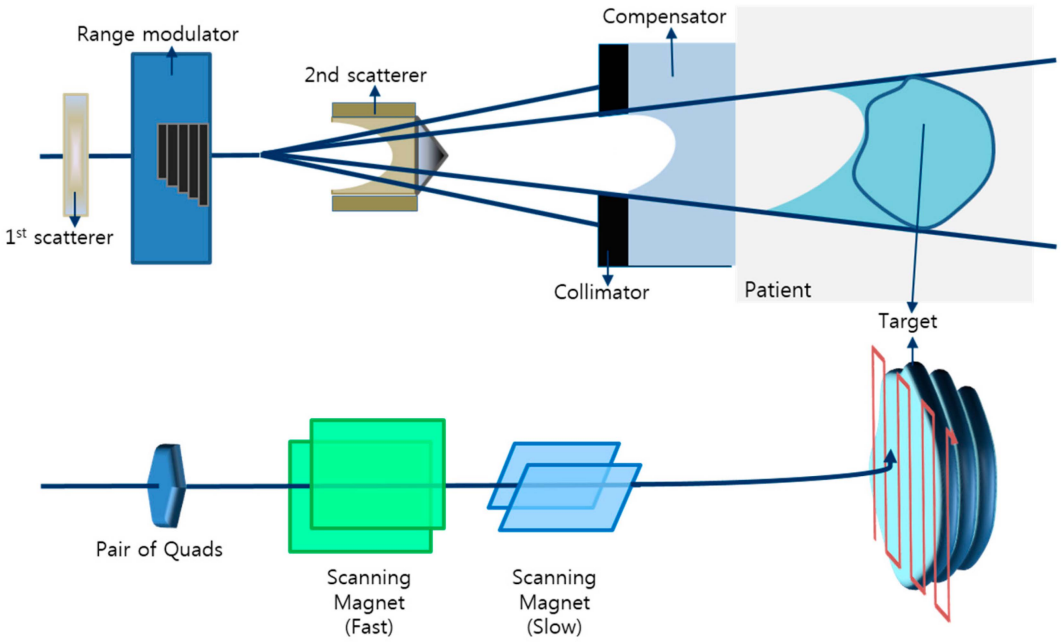

Fig. 4. Proton beam delivery techniques: Passive scattering mode (upper panel) and PBS mode (lower panel). From [45], used under the creative commons attribution (CC BY) license.

treatment time by performing the filling of the synchrotron more efficiently or by extracting multiple beams of different energies within the same machine cycle [41]. The latter can be done by changing the current patterns of the power supplies of the main bending and quadrupole magnets such that they contain extended flattops for beam extraction, combined with a stepwise pattern of short flattops for fast energy changes. Technological developments in carbon therapy accelerators are pursued by two vendors: 1) Toshiba (Tokyo, Japan) and 2) Hitachi (Tokyo, Japan).

C. Other Technologies

The ideal characteristics of an accelerator for particle therapy are a small size and a low weight, easy and reliable operation, low-capital and operational cost, variable beam energy, small beam losses, fast dose delivery, capacity for increased beam current (e.g., for FLASH therapy), fully achromatic transport, and access to a variety of particles ranging from protons, He, C, O and Ne.

Alternative solutions to cyclotrons and synchrotrons have been investigated, all pointing at lower cost and more compact designs. Linac-based designs are being investigated since more than a decade [42]. A compact and modular design has been developed by advanced oncotherapy—application of detectors and accelerators to medicine (AVO-ADAM), Geneva, Switzerland, that is currently being installed and commissioned. The major advantage of linear designs is the faster energy change. Recently an energy of 230 MeV has been reached for the first time. Another technology under development is the fixed-field alternating gradient accelerator (FFA) [43]. These machines are circular accelerators, characterized by time-independent (fixed) magnetic fields together with an increased focusing strength achieved using the "alternating-gradient" principle. The main advantages of such systems is that the magnets are simpler to construct and operate and that the average output current can be higher. Recently a proof-of-principle proton FFA accelerator was built at KEK and a prototype model for medical applications with protons up to 150 MeV was successfully commissioned [44]. Other systems that are under study are laser-plasma accelerators and dielectric wall-accelerators, that will be discussed briefly in Section VII.

III. Beam Transport and Delivery Techniques

A. Dose Delivery Techniques

Before discussing the technical developments in beam transport, it is useful to summarize the two major techniques by which the prescribed dose is delivered to the tumor volume. The difference between the techniques is displayed schematically in Fig. 4, which is taken from [45] discussing proton therapy. This could be generalized to particle therapy.

1) *Passive Scattering:* This technique has been in use since the 1950's and was up to a decade ago the most commonly employed proton delivery technique. The standard used technique is double scattering, applying a combination of low and high-Z materials. A proton beam hits a scatter foil, usually made of a high-Z and high-density material, spreading the beam laterally. The beam is further shaped via field-specific apertures (collimators) that are placed in the beamline. They are typically made of dense high-Z materials, such as solid brass or metal alloys, to maximize proton stopping within a short distance. Composite materials have also been investigated [46]. Beam depth is manipulated via a modulation wheel, which produces the varying energies needed to treat the entire target under the spread-out

Bragg peak (SOBP). This is usually done with low-Z materials to limit scattering (see also Section III-B). The beams are further shaped to conform to the distal edge of the tumor (typically using low-Z compensators) to account for both tissue inhomogeneity and tumor shape. The main disadvantage of passive scattering is the associated secondary stray radiation, which leads to activation of the beam-modifying devices, the environment, and the patient. Another disadvantage is the dose conformity: while the distal dose conformity is excellent, the proximal dose conformity is low (see Fig. 4 top). Finally, for each patient individual hardware is needed (compensators and collimators). Current research efforts in passive scattering are aiming at optimizing the design and beam shaping materials [47], [48].

2) *Active Scanning:* Two modalities can be distinguished. The first one is spot-scanning or PBS. This technique has been first employed at PSI in Switzerland [49]. The beam has typically a small width (a few mm at the isocenter) and its energy is variable. Along the lateral directions the beam is deflected by scanning magnets. In case of a gantry, these are located before (upstream scanning) or after (downstream scanning) the final bending magnet. The position in depth of the Bragg peak can be chosen by setting the beam energy, allowing for an excellent dose conformity. The advantage with respect to passive scattering is the higher-dose conformity and the significant reduction of the amount of stray radiation. Additionally, PBS offers the possibility of intensity modulated proton therapy (IMPT) and intensity modulated carbon beam therapy (IMCP). Particle beams with varying energy and position are delivered here, requiring magnetic field ramp rates of up to 250 T/s [50]. Thanks to major technological advances in the development of fast scanning magnets and their power supplies, today PBS is the most widely used method for particle therapy dose delivery. The second active scanning modality is uniform beam scanning. Here, a range modulator, a patient collimator and range compensators are required, similarly to the passive scattering technique, but it utilizes magnets instead of scattering foils to spread the beam laterally. The beams are scanned in a fixed pattern with a uniform intensity. The amount of stray radiation is smaller than in passive scattering.

Passive scattering has been the main delivery technology for many years. It is a robust and reliable delivery technique, and much clinical experience has been gained. New centers mostly chose PBS because of the higher flexibility for target conformity. Some comparison studies performed for protons suggest clinical differences between passive scattering and active scanning (see for instance [51]). For example, there are differences in linear energy transfer (LET) distributions, in relative biological effectiveness (RBE), and in dose rate, possibly explaining different treatment outcomes. Technological developments are mainly regarding the PBS technique, and many of them aim at achieving faster scanning speeds, smaller spot sizes, and more accurate spot positioning [52], [53]. An emerging technology for dose delivery is arc therapy, where a spot-scanning beam is delivered while rotating the gantry. We come back to this technique in Section VII.

B. Energy Selection System

Energy selection systems are needed to modulate the beam energy in proton therapy facilities that make use of cyclotrons and synchrocyclotrons and offer active scanning. An energy selection system consists of an energy degrader, i.e., an absorber of variable thickness, followed by a series of dipole magnets and collimators. Regarding the degrader, this should be made of a low-Z material, so that the radiation length is small and multiple Coulomb scattering is reduced. Moreover the density should be high so as to have a larger stopping capability.

The material should also have high-beam transmission efficiency to minimize beam loss and production of secondary particles. The most widely used materials are graphite and beryllium, but research is ongoing toward composite materials, such as B_4C with graphite [54], that have better-transmission efficiency with respect to pure materials. Some research is also ongoing to find an optimal shape. Typically they are wedge-shaped, but parallel-sided degraders and single block degraders have also been recently proposed [55]. Dipole magnets and collimators located downstream the degrader can be used to limit the energy spread in the beam and to define the emittance and transverse beam distribution. An example of a modern energy selection system currently in use at the PROSCAN facility at PSI is shown in Fig. 5: after the degrader there are two collimators (C1 and C2) that limit the emittance of the beam, whereas the energy/momentum selection is done by the dipole magnets (D1) and the slits [56].

A disadvantage of the energy selection system is the associated beam losses, which become larger with lower-beam energies. They can be as large as 99% of the primary protons, when the beam is degraded from 250 to 70 MeV [57]. The system and all the surrounding components get heavily activated. New techniques to increase beam transmission by reducing the momentum spread of the beam have been investigated recently at PSI [58]. Another disadvantage is the non-negligible time it takes to switch energies. Advances in technologies have resulted in energy selection systems in cyclotron facilities that typically switch energy in about 1 s [59].

C. Beam Transport and Gantry

From the accelerator the particle beam has to be transported to the treatment room. For proton treatments, energy variations between 50 and 250 MeV may be necessary, and for carbon treatments the energy variations may be from 80 to 430 MeV/u. Beam transport systems require fast changes in dipole magnet strength (sweep rate), with values up to a few hundred mT/s. The final section of the beamline can be fixed, or it can be a system that can rotate around the patient ("gantry"), preferably up to 360 degrees. A rotating gantry is clinically strongly desirable [60] so that the patient can be treated in supine position, i.e., the same position as used

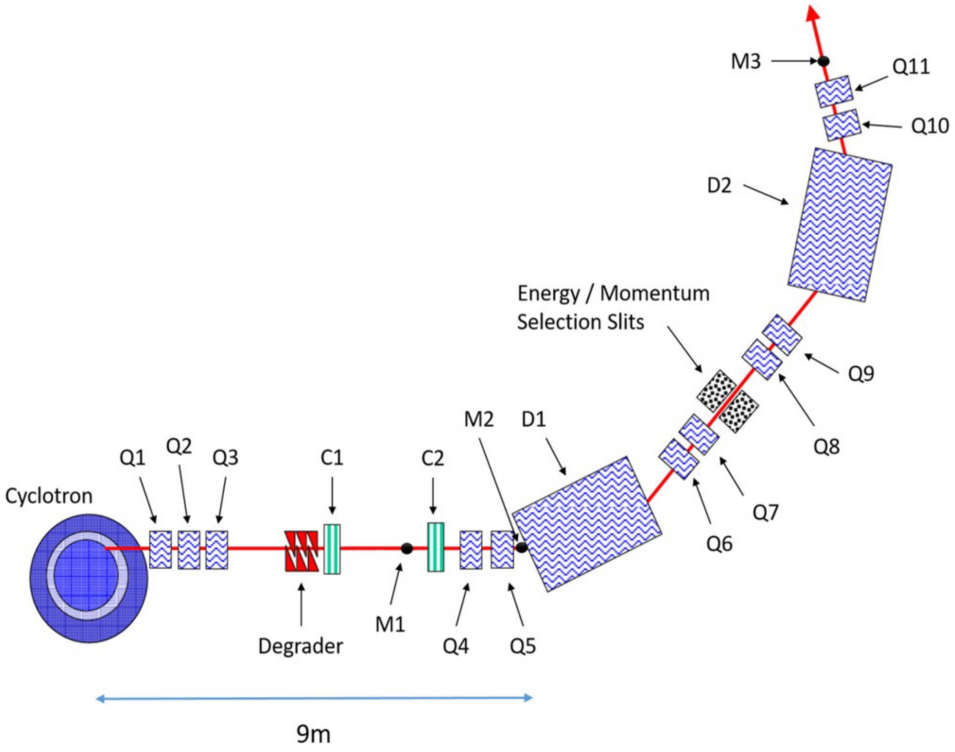

Fig. 5. Illustration of the energy selection system of the PROSCAN beam line at the PSI. (Q = quadrupole magnet, D = dipole/bending magnet, C1 = beam size selection collimator, C2 = beam divergence selection collimator, and M= beam current and beam profile monitor). From [56], used under the creative commons CC-BY-NC-ND license.

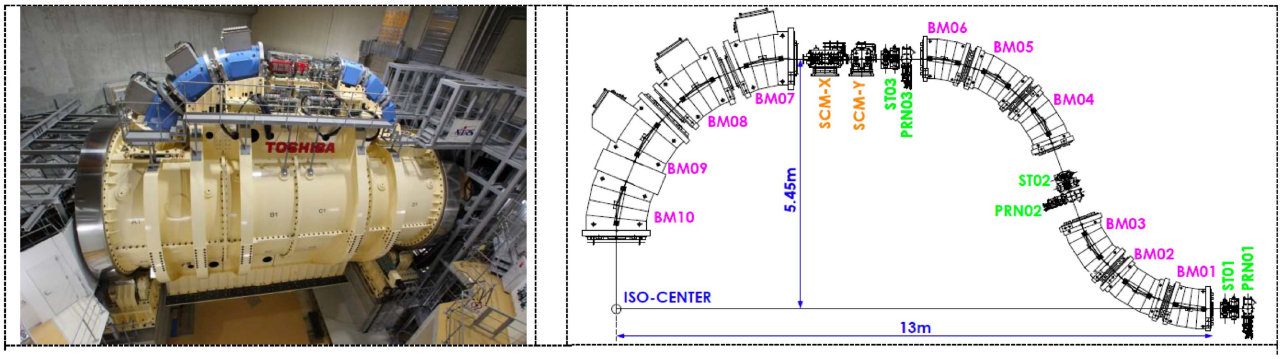

Fig. 6. Left: Schematic layout of superconducing rotating gantry at NIRS for carbon ion radiation therapy. Right: Layout of the superconducting rotating-gantry, with ten superconducting magnets (BM01–BM10), a pair of scanning magnets (SCM-X and SCM-Y), three pairs of beam profile-monitor (STR01–STR03), and steering magnets (SCN291–SCN293). From [68], used under the creative commons attribution 3.0 license.

for diagnostic scans. Moreover, a rotating gantry provides the maximum flexibility in selecting the irradiation direction.

Gantries represent a major cost because of their large size and weight. Proton therapy gantries based on normal conducting magnets have typically a weight of 100–200 tons and are more than 10 m in diameter. Gantries for carbon therapy are even larger: the normal-conducting gantry at the Heidelberg Ion-Beam Therapy Center (HIT) has a weight of 600 tons and a diameter of about 15 m [61]. The installation of such a large and complex system poses technological problems, and the associated costs are high. Therefore, technological developments aim at reducing the footprint of these systems.

Superconducting high-field magnets can be used to develop more compact gantries. The main challenges in the usage of such strong field magnets (typically several T) are magnet quenching, ramping time, and the complexity of the cooling systems needed. Reviews about superconducting gantries can be found in dedicated works [4], [62], [63], but we highlight a few developments here.

For proton therapy, superconducting gantries are already in use. The 25 tons SC360 superconducting proton gantry by ProNova Solutions has been commissioned and clinically applied in a few facilities worldwide [21]. Here, a series of dipoles and quadrupoles are arranged sequentially ("combined-function") to bend the beam achromatically. Similarly, Nesteruk et al. [64] proposed a gantry with larger energy acceptance and faster energy change time, using dipole, quadrupole and sextupole magnets.

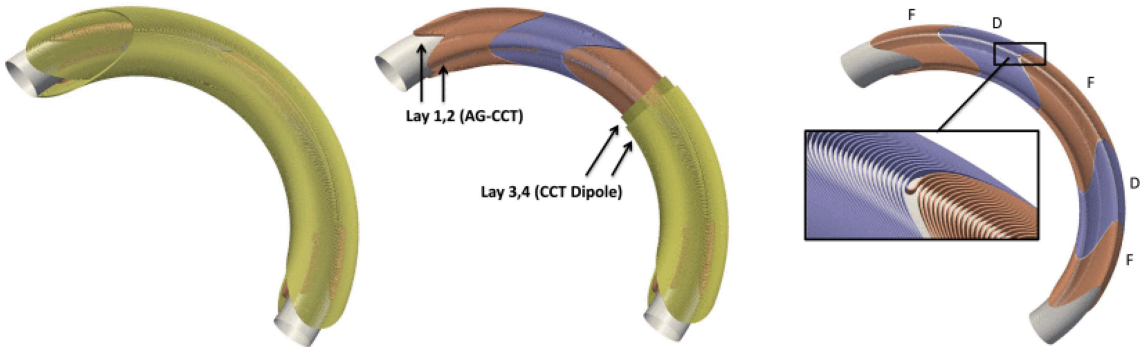

Fig. 7. Design of an achromatic superconducting CCT magnet. Left: Outer view of four conductor layers; Center: View with the dipole cut back to show the inner pair of alternating gradient-CCT layers; and Right: Inner layer consisting of a CCT quadrupole with the current reversal between a focusing (F) and defocusing (D) section. Reproduced from [70].

Regarding carbon therapy, the first superconducting gantry in the world was installed and commissioned at NIRS in Chiba, Japan [65]. The system, shown in Fig. 6, has a weight of 300 tons, a length of 13 m and has treated the first patients in 2017. Just like the above mentioned superconducting proton gantries, it is based on a series of dipoles and quadrupoles. A more compact version of this gantry with a reduction of about 2/3 in size and weight is in preclinical commissioning at Yamagata University and a rotating gantry of the same type is to be installed for the Yonsei University Health System (Seoul, South Korea) and Seoul National University Hospital (Seoul, South Korea) [66]. An even more compact version is being designed in collaboration with Toshiba (Tokyo, Japan) [67]. One of the main challenges is the cooling of superconducting magnets (4 K). Gantry magnets that can be operated at higher temperature (77 K) are also being investigated [68].

The above mentioned gantry designs make use of superconducting magnets arranged sequentially, each with coils wound according to conventional winding schemes, i.e., the superconducting wire is wound around a coil form (racetrack or saddle point winding). Superconducting magnets with other winding schemes have also been explored. The "canted cosine-theta" (CCT) magnets (or tilted double helix magnets), conceived in the 1970s [69], have been revived in the last decade. The idea is that an overlaid pair of solenoidal coils tilted in opposite directions generates a dipolar field normal to the solenoidal axis. For a quadrupole the structure is slightly more complex. If these configurations are used in a bending geometry, these magnets can be used in gantries to bend the beam. Recently several innovative magnet designs based on this concept were studied, such as the achromatic alternating-gradient superconducting magnet by Brouwer et al. [70], that is shown in Fig. 7. The rotation of heavy structures as required in gantry designs is mechanically challenging, as discussed by Piacentini et al. [71]. A design for operation in a steady-state without rotation is the GaToroid gantry for protons and heavier ions [72], that makes use of a toroidal field configuration.

D. Gantry Free Transport Lines

The high-installation costs associated with the beam transport has fueled discussions about whether a gantry is actually needed. Recent studies state that a gantry is not strictly needed for a large group of patients [73], [74]. The work by Volz et al. [75] discussed the economical and clinical advantages for an upright patient positioning system, as well as advances in the design of chair systems and associated image guidance systems. An upright positioning system could also naturally provide an efficient way for advanced beam delivery options, such as particle arc therapy [76], because the patient can easily be rotated. Various technological developments are therefore ongoing in the chair design of these systems, examples of which can be found in various works [77], [78]. Sun et al. [79] described the clinical implementation of a chair positioning system for head and neck cancers at the Shanghai Proton and Heavy Ion Center, showing a study of positioning accuracy and a dose comparison between the chair and the supine arrangement. Gantry-free dose delivery systems could be the solution for a more widespread access to particle therapy also in low-income countries, reducing cost and size of particle therapy centers. Although a large fraction of patients can be treated without gantry [73], the above works also acknowledge that patient comfort is also important and not all patients can be treated this way, including anesthetized patients, such as children. Thus, it is not expected that the gantry can be fully eliminated.

E. Beam Monitor Systems

The final part of the beam delivery system is the beam monitoring system that monitors the accurate delivery of the dose. The typical requirement of such a system is that it can online measure particle fluxes of 10^6–10^8 particles/s with a read-out frequency of at least a few kHz. There is a large variety of detector technologies to monitor online the intensity and positioning of the beam. A dedicated review to beam monitoring systems is provided by Patera and Sarti [80], containing also an overview of detectors used for dosimetry and microdosimetry. The most widely used technique for beam monitoring is that of ionization detectors, exploiting the ionization produced by the beam in a gaseous medium. Other techniques are solid state detectors, scintillating and optical fiber detectors, and secondary electron emission detectors. Dosimetry measurements are widely made with calorimeters, ionization chambers, and Faraday cups, but other detector technologies are coming up, including diode detectors and

passive alanine detectors. Microdosimetry measurements are aiming at investigating the microscopic distribution of the deposited dose in volumes of (sub)-cellular dimensions. These measurements are mostly done with gas counters called mini-TEPC (miniaturized tissue-equivalent gas-proportional counters of 1 μm of equivalent size). Thin silicon detectors of 1–2-μm thickness, thick silicon detectors of 10 μm or larger, and 2-μm thick diamond detectors are also used (see [81]).

IV. Developments in Monte Carlo Simulations

Thanks to the accurate tracking and simulation of interactions of particles in complex geometries, the MC technique has become an important calculation tool in particle therapy, bringing benefit to quality assurance (independent dose calculations), dosimetry, radiobiological modeling, design and commissioning of clinical facilities, shielding, radiation protection, commissioning of treatment planning systems (TPSs), and development of range monitoring strategies. This section summarizes developments in the MC modeling that is relevant for dose calculations, focusing on general purpose codes based on the condensed history approach, such as GEANT4 [82], FLUKA [83], [84], MCNP [85], SHIELD-HIT [86], PHITS [87], and SRIM [88]. These codes are complex to use, and user-friendly platforms to facilitate their use have been developed, including TOPAS [89], PTSIM [90], and GATE [91] for GEANT4. An example of an accelerator tracking code with particle–matter interactions is BDSIM, based on GEANT4 [92]. Below we will also discuss how the general purpose MC codes are coupled with biological models.

A. Nuclear Physics Modeling in MC Codes

Charged hadrons of energies as necessary in particle therapy (up to a few hundreds of MeV/u) interact in tissue by electromagnetic and nuclear interactions [93]. Modeling of electromagnetic interactions is complex but usually considered sufficiently accurate. However, nuclear physics models are not considered fully satisfactory [10]. They have an important impact on physical dose: inelastic interactions cause beam attenuation build up of secondary ions, and elastic interactions contribute to beam broadening. [10], [94], [95]. Moreover the effects on biological dose are substantial due to the production of secondary fragments [96]. Many efforts have been done in modeling transport and interactions of charged hadrons in MC codes [10]. This has lead to excellent agreements in longitudinal and lateral physical dose distributions between dose measurements and MC simulations (see for instance [97], [98]). At the same time, several disagreements were found between data and MC predictions, mostly related to hadronic models. We highlight a few examples.

1) *Physical Dose for Primary Particles Other Than Protons and Carbon Ions:* For example, significant discrepancies were reported between FLUKA and measurements in lateral and longitudinal dose of helium atoms in water [99]. These differences were attributed to an underestimation of the contributions to physical dose by secondary particles produced at large angles. Recently, new cross-section measurements for fragmentation of helium have been done [100], as shown in Fig. 8. The hadronic models in FLUKA were updated with these measurements for fragmentation of helium ions, thus reducing the disagreement [101].
2) *Production of β^+ Emitting Nuclei From Nuclear Interactions Between the Primary Particles and the Medium, Used for Range Monitoring Purposes (See Section VI-A1):* General purpose MC codes are able to predict the yields and spatial distributions of the most abundantly produced species as ^{11}C or ^{15}O with sufficient accuracy, but more efforts are needed to predict spatial distributions of nuclides with short lifetimes, such as ^{10}C or ^{12}N [10]. Fig. 9 shows the cross section data from the EXFOR library for the production of ^{11}C and ^{15}O. Discrepancies between the various experiments are well visible. Several recent efforts have been done to collect new data and improve the hadronic models for short-lived β^+ emitters [102], [103], [104].
3) *The Emission of Prompt Gammas (PGs), From the Final Stage of a Nuclear Reaction (See Section VI-A2):* Disagreements were reported between measurements and the GEANT4 in the prompt-gamma energy spectrum, yields and spatial distributions [105], [106], [107]. Modeling PG emission is challenging, because it is influenced by the nucleus spin and parity, and because the shape of emission lines is subjected to Doppler broadening due to nuclear recoil. More research is needed to improve PG production models.
4) *Production of Secondaries in Target and Projectile Fragmentation Reactions (See Section VI-A3):* Regarding MC simulations, there is a lack of experimental data for fragment emission at large angles. Such data are important for benchmarking the hadronic models. The FOOT experiment aims at providing new differential cross section measurements [108].

B. Radiobiological Modeling With General Purpose MC Codes

General purpose MC simulation codes generally follow a condensed-history approach, where the cumulative effects of multiple particle collisions is modeled. The free path length, the energy lost and the deflection are all sampled stochastically and nuclear reactions, including secondary particle production, are modeled according to their cross sections. These codes are appropriate tools to calculate quantities as radiation dose for volumes, such as the human body.

However, to estimate radiobiological effects in the human body, such as DNA lesions or cell death, much smaller scales should be considered, and general purpose MC's are not the most appropriate tools. Instead, this can be better performed by means of track structure codes, which are developed to simulate all single collisions with atomic electrons in the target in an event-by-event manner. The outcome of the simulation is a set of spatial coordinates of ionizations and excitations, induced by the primary particle and its secondary electrons, as well as energy depositions in each event, forming the particle

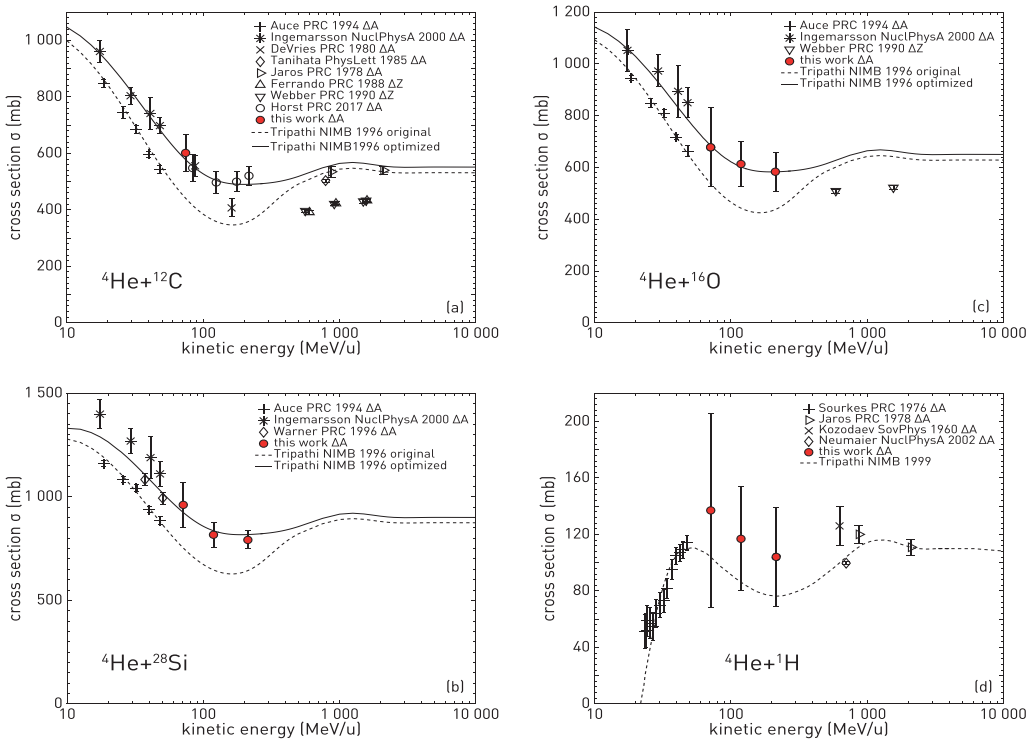

Fig. 8. Recent cross section measurements from Horst et al. [100], with in red the new measurements of the mass-changing cross sections for ^{4}He ions on C (top left), O (top right), Si (bottom left), and H (bottom right) targets, compared with other data and with two cross section parameterizations. From [100], used under the creative commons attribution 4.0 international license.

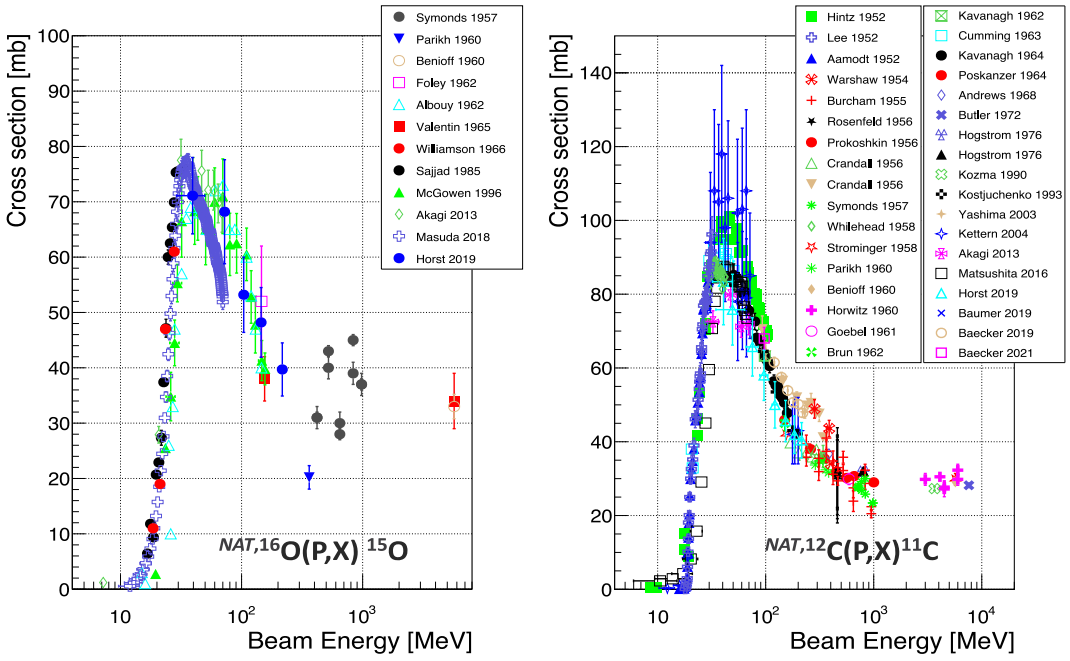

Fig. 9. Experimental measurements of the two most abundant β^{+} emitters produced by proton interactions as a function of the projectile energy: ^{16}O(P,X)^{15}O (left) and ^{12}C(P,X)^{11}C (right).

track [109]. Not only physical, but also physico-chemical and chemical processes can be modeled. A comprehensive overview of MC track structure simulation codes in particle therapy is presented by Rucinski et al. [110].

A recent approach aiming to merge the track structure approach into the framework of a general purpose MC code is the GEANT4-DNA project [111]. This code allows to implement the geometry of biological targets at nanometric scales, such as the DNA molecule, and can model the interactions of electrons and ions, including hydrogen and helium isotopes, down to the eV scale. Another MC framework that has merged a track structure approach into a general purpose MC is

TOPAS-nBio [89], [112], which can model radiobiological effects at the nanometer scale. Both codes allow to couple chemistry models to simulate indirect effects of radiation, such as the production of radicals.

Track structure codes perform calculations on microscopic/nanometric volume scales, making their application in simulations of treatment plans on a spatial scale of a human body impracticable. To estimate radiobiological effects in large volumes, such as the human body, a commonly used approach is to calculate a dose distribution weighted with the RBE, D_{RBE}. For an extensive review about radiobiological modeling we refer to Tinganelli and Durante [8].

Two biological models have been developed to calculate RBE: 1) the local effect model (LEM) [113], [114], used at European carbon–ion centers and 2) the microdosimetric kinetic model (MKM) [115] used at the Heavy Ion Medical Accelerator in Chiba, Japan. A common approach in MC simulations to evaluate the RBE-weighted dose (D_{RBE}) is to exploit the survival probability S of cells as function of physical dose D as predicted by the Linear Quadratic model [116], that provides a simple relationship between cell survival S and delivered physical dose D

$$S = e^{-\alpha D - \beta D^2}. \tag{1}$$

Here, α and β are parameters that depend on several variables, such as the tissue type, particle type, energy, dose, and LET. For a given survival level S the RBE is defined as

$$\mathrm{RBE} = \frac{D_x}{D_i} = \frac{2\beta_i\left[-\alpha_x + \sqrt{\alpha_x{}^2 - 4\beta_x \ln S}\right]}{2\beta_x\left[-\alpha_i + \sqrt{\alpha_i{}^2 - 4\beta_i \ln S}\right]} \tag{2}$$

where α_X and β_X are the coefficient for photons, while α_i and β_i are the coefficients for the ions of interest i. By calculating the RBE in each voxel, and multiplying the physical dose D by the RBE value found in that voxel, a D_{RBE} distribution can be obtained.

Both GEANT4 and FLUKA can calculate D_{RBE} as reported by Kase et al. [117] and Battistoni et al. [84], respectively. In both cases, dose-weighted average values for α and β were obtained from precalculated databases for different tissue types and particle energies. This allows to simulate the cumulative effect of the mixed radiation field (all primaries and secondary particles), yielding the total RBE and D_{RBE} in each voxel. At CNAO, the FLUKA framework was also coupled to the MKM model from NIRS, and used for clinical dose calculations [118].

Another recent development in the coupling of radiobiological models with general purpose MC regards the BIophysical ANalysis of Cell death and chromosome Aberrations (BIANCA) model [119]. This model takes into account the development of complex DNA lesions, chromosomic aberrations and their capability of inducing cell death. Recently, the BIANCA code was coupled with FLUKA, allowing to calculate RBE and D_{RBE} voxel-by-voxel [120].

Finally, a MC-based computational framework for the calculation of several physical and biological irradiation quantities is PlanKIT [121]. It is based on the FLUKA MC code and the implementation allows to produce universal Look-Up tables of physical and radiobiological quantities, such as dose, track-averaged, and dose-averaged LET, and by coupling to the MKM radiobiological model, α and β coefficients to derive RBE according to the linear-quadratic model. The application into a treatment planning workflow for spot-scanning was also discussed.

C. Fast MC Simulations

It has been demonstrated repeatedly that MC calculations have a much larger accuracy compared to analytical pencil beam (PB) algorithms in heterogeneous tissues or complicated geometries (see for instance [122]). Being considered as gold standard for dose calculations, MC simulations are often used to verify dose distributions of commercial TPSs, that are typically based on analytical dose algorithms. This is done, albeit not routinely, by recalculating treatment plans from commercial software with MC simulations, and comparing them. An obvious difficulty in the routine application of MC codes is the large amount of computing resources that is required for an accurate MC simulation of a treatment plan: it can take several hours to simulate a multifield proton therapy treatment plan on central processing unit (CPU) [123], and even more for a carbon therapy plan. This is more than what is clinically acceptable (less than 30 min). The reason is that simulating a particle treatment plans requires transporting large amounts of particles: a typical proton therapy plan contains 10^{10}–10^{12} protons, and for carbon therapy a factor 10^2 below, depending primarily on target volume [124]. Computation time can be reduced by running parallel independent histories on a cluster of CPUs, but this is not straightforward for all therapy centers. Much research has therefore focused on the development of fast MC techniques. We highlight various initiatives in the next section.

1) MC Simulations on GPU: The usage of graphics processing units (GPUs) has turned out to be an effective way to speed up MC simulations. Advantages and challenges in the usage of GPU in dose calculations are discussed in an early reviewed by Jia et al. [125]. A rapid evolution in the application of GPU has taken place since then, partly documented in [10] and updated below.

For proton therapy various GPU-accelerated MC proton PB dose engines have been developed for research purpose in the last decade, including fast particle therapy dose evaluator (FRED [126]), GPU-based MC code (gPMC [127]), simplified MC code (SMC [128]), MOQUI for QUIck proton dose calculation [129], see Fig. 10), GPU-accelerated MC dose (GPUMCD [130]), and a fast MC dose engine including detailed modeling of elastic and nonelastic proton–nucleus collisions [131]. A GPU-accelerated 4D dose calculation framework that includes effects from dynamic dose delivery is reported by Pepin et al. [132].

For carbon therapy various GPUMCD engines were developed as well, including FRED [126], [133] and GPU OpenCL carbon MC (goCMC [134]). Fig. 11 shows the longitudinal and lateral dose profiles as predicted by the FRED fast MC framework, compared with FLUKA simulations.

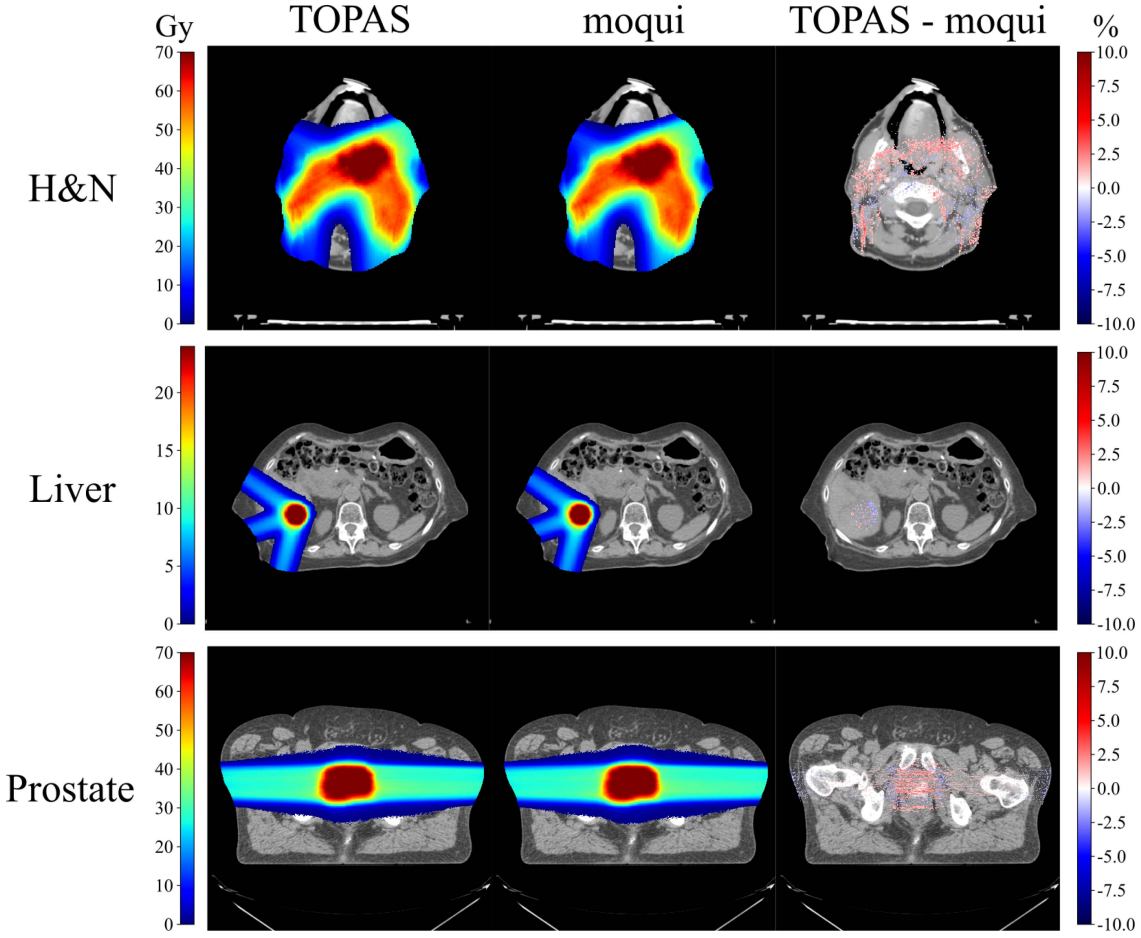

Fig. 10. Comparison between calculated dose by the full MC code TOPAS (left panels), the GPU-accelerated code MOQUI (center panels), and the difference between them (right panels), for a head- and-neck case (top), a liver case (middle), and a prostate case (bottom). Good agreement was found between them. Figure courtesy of H. Paganetti.

These kind of comparisons with full MC codes are essential to ensure accuracy.

Finally, simulations of radiobiological effects with the help of track structure codes can also profit from GPU-acceleration [135], [136], [137].

2) Other Methods to Accelerate MC Simulations: Besides GPU, other approaches have been developed to accelerate MC dose simulations, reviewed in detail by Muraro et al. [10]. First, phase-space files can be used, that contain parameterizations of physical properties (energy, direction) of the primary particles that exit a treatment head [138], leading to much faster MC simulations. This was also used in recent work by Lysakovski et al. [139], presenting a fast MC dose engine (MonteRay) running on CPU for proton therapy calculations at HIT. It includes magnetic field support for the purpose of MR guided ion therapy. The code was recently extended to include also helium and carbon transport and interactions. In this later version the phase space approach was replaced with a model of the HIT beamline together with a parametrization of the beam [140]. Second, MC dose calculations can be accelerated with track-repeating algorithms [141], [142], where pregenerated events are used during simulation to accelerate dose calculations. Initiated two decades ago, this technique was used for clinical application at the Shanghai Proton and Heavy Ion center [143]. An extension to carbon therapy has also recently been developed [144]. Other methods to speed up dose calculations include: voxel-MC algorithm [145], macro-MC algorithm [146], virtual particle MC simulations [147], and an equivalent restricted stopping power (SP) MC [148].

Fast MC-based dose kernels have also been introduced into commercial TPSs. For instance, the RayStation TPS (Raysearch, Stockholm, Sweden) provides the user the possibility to perform forward MC dose calculations for protons, based on a condensed history MC for primary and secondary protons [149]. This MC dose engine has been validated in clinical context [150]. Moreover, the Eclipse TPS now provides users a MC dose algorithm for proton therapy (AcurosPT) [151].

V. Treatment Planning

TPSs are a key component of particle therapy treatments to ensure that the tumor tissue receives the maximum therapeutic dose while sparing surrounding tissue and critical organs as much as possible. Advancements in particle therapy treatment planning have come primarily in the form of innovative hardware (target imaging, immobilization devices, dose delivery, etc), planning strategies (robustness, combination

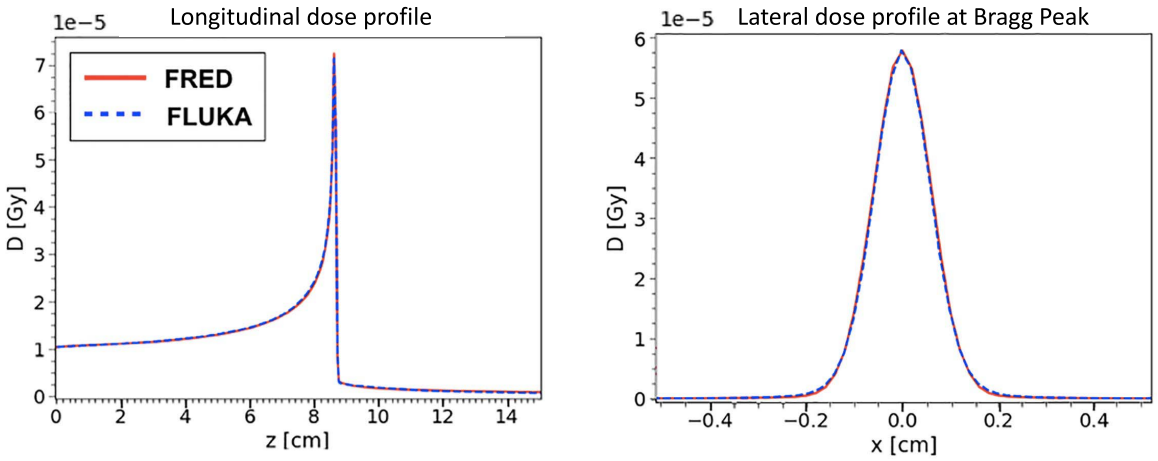

Fig. 11. Absorbed dose in water for a 200-MeV/u carbon ion beam simulated with the GPU-accelerated MC code FRED (red continuous line) and the general purpose MC code FLUKA (blue dotted line). Left: Longitudinal dose profile (integrated transversally). Right: Lateral dose profile at 8.6-cm depth, which corresponds to the maximum value of the dose, at the Bragg peak. A very good agreement can be seen. From [133], used under creative commons attribution license (CC BY).

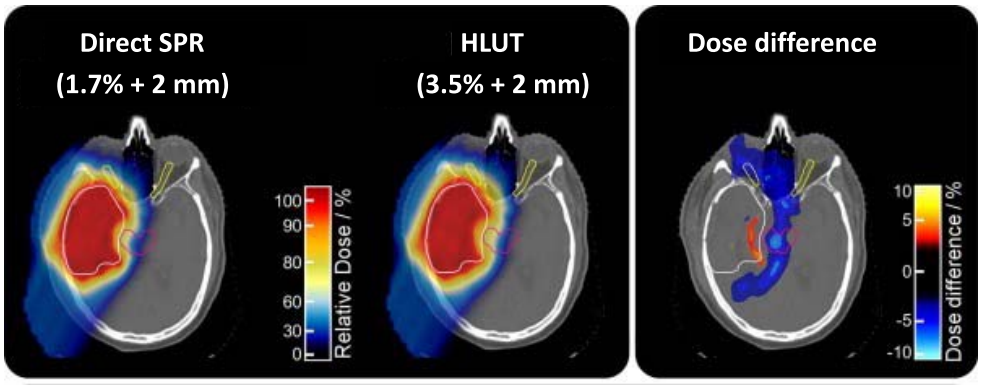

Fig. 12. Clinical treatment plan of a representative glioblastoma patient calculated using the DirectSPR method with the reduced range uncertainty margin (1.7% + 2 mm) thanks to dual energy CT (left) in comparison to the conventional method using hounsfield look-up tables (HLUTs) with the old clinical margin (3.5% + 2 mm) (middle). The prescribed dose to the target was 60 Gy. From [158], used under the creative commons CC-BY-NC-ND license.

of fields, spot placement strategies, etc), and computing technologies (algorithms, etc). Concerning imaging techniques for treatment planning, these are based on the same technologies as those employed in conventional radiotherapy (see for instance [152]). Topics about planning strategies are more appropriately described in more clinically oriented works (see for instance [153], [154]). In this section we discuss aspects regarding treatment plan computations. The focus is on research where MC simulations played an important role in their development and validation. Following the components in a particle therapy treatment plan computation, we highlight several developments.

A. Patient Geometry and Beam Model

The physical modeling of the patient needed for a treatment simulation is based on the CT scan, where the attenuation of photons is measured with a dimensionless quantity known as hounsfield units (HUs). For particle therapy dose calculations, HUs must be converted to SP. The most commonly applied method for this scope is using stoichiometric calibrations [155]. This approach leads to inaccuracies in range up to 3.5% [156]. It has been demonstrated that dual-energy CT (DECT) improves the accuracy of the conversion (see for instance [157], [158]), but is not yet widely utilized in treatment facilities. Fig. 12 shows how the usage of dual energy CT leads to a reduction of dose to the tissue surrounding the tumor.

The definition of the clinical target volumes (CTVs) follows the same strategies as those used in conventional radiation therapy, but the impact of uncertainties can be larger in particle therapy. Magnetic resonance imaging (MRI) has been suggested as solution to improve target definition in particle therapy, better depicting the soft tissues. One of the difficulties here is how to co-register the CT and MRI scan. AI techniques have been proposed for this scope [159]. Apart from co-registration AI is today applied in many other aspects in radiotherapy that regard target definition (contouring/segmentation, image reconstruction, image registration), as extensively described in the reviews about AI in radiotherapy [160], [161] and particle therapy [15].

Accurate treatment plan simulations require a careful characterization of the initial shape and characteristics of the particle beams in terms of energy, beam size, divergence, and

emittance (and uncertainties therein) [162]. These are influenced by the accelerator and beam transport system. Various works are available that describe the development of treatment room specific beam models. Examples of beam modeling with TOPAS, GATE, FLUKA, and PTSIM are described in [97], [163], [164], and [165], respectively. The modeling of a specific beam line is a complex and time-consuming work. Fuchs et al. [166] have recently developed a computer-driven method, allowing for a simple and straightforward generation of a MC beam model of a scanned proton and carbon ion beam delivery system.

B. Dose Calculations

To compute the dose in the patient, a dose calculation engine is used. In the last decades various algorithms have been developed for particle therapy, reviewed for instance by Saini et al. [167]. The most widely used algorithms can be classified into two main categories: 1) MC methods, as discussed in Section IV and 2) PB algorithms. Here, the dose is calculated based on the convolution of 3-D undisturbed proton fluences in air with a "beamlet" in water. The latter are based on precalculated models of absorption of dose in water, that should be validated with MC simulations and in-house measurements [168]. Many of the currently available PB dose calculation algorithms used in clinical practise today are based on the analytical algorithms developed by Hong et al. [169] and Schaffner et al. [170]. These algorithms provide fast computation, but at the expense of lower-dose calculation accuracy in the presence of tissue heterogeneity [171], [172]. This is mainly because these algorithms adopt approximations that disregard lateral inhomogeneities, and moreover Multiple Coulomb Scattering and nuclear interactions are modeled in an approximate way. In particular for lung patients it was noted that more accurate algorithms like MC are urgently needed [172]. However, continuous improvements of the analytical models are ongoing. An example is the fast dose recalculation on GPU (FRoG) dose engine [173], [174], that can be used for dose calculations with protons and other ions. Fig. 13 shows a treatment plan for protons (left) and helium ions (right), where the reduction of dose in tissues surrounding the tumor can be clearly seen. It can also estimate radiobiological quantities, such as dose-averaged LET, and allows comparing D_{RBE} with the LEM and MKM model. The dose algorithm has an accuracy close to MC.

As alternative to the above two categories, deep learning methods have recently been considered. The feasibility to use convolutional neural networks (CNNs)-based dose calculation methods was investigated for proton therapy [175]. Here, the 3D-CNN model learned the volumetric proton dose distributions for every spot beam from a large set of training data. The model could accurately calculate 3-D dose and associated uncertainties.

CNNs have also been proposed to convert PB dose to MC dose [176]. By using CTs and PB calculated dose distributions of hundreds of patients, the authors showed that large improvements in the accuracy of PB dose could be achieved, similar to that of MC dose.

C. Optimization

1) Physical Dose-Based Optimization: The development and widespread use of PB dose delivery systems has lead to the development of new treatment planning techniques, in particular "inverse" optimization. Here, a series of final dose goals are set by the radiation oncologist and planner, and the most appropriate PB weights are calculated to obtain the most optimal dose distribution, as opposed to "forward" treatment planning referring to the technique where preselected PBs are used and the dose distributions are calculated [177], [178]. For a detailed description about treatment optimization we refer to the comprehensive review by Moore [179], and we just discuss the main concepts here.

Starting with a dose prescription and a set of dose limits for critical organs, optimization is the calculation process to identify a set of PB intensities that is expected to best realize the clinical objectives in terms of target coverage and OAR dose. The treatment goals are formulated as a set of objective functions. Optimization is typically done by minimizing an overall objective function to obtain an optimal solution of the PB weights. Usually, the PBs are placed according to a cubic or hexagonal pattern to cover the tumor, but other options like randomly places beams or combining beams of different sizes have been investigated [180]. In treatment plan optimization many iterations are typically needed for the objective function value to evolve toward a minimum, and the physical dose must be recalculated for each iteration, making optimization a computationally expensive process, especially for MC-based calculations.

In most clinically used TPSs optimization is based on analytical dose algorithms. However, with the availability of fast MC codes and the growing consensus that MC calculations are more accurate than analytical PB algorithms, interest has grown to include MC calculations also in inverse dose computations. One of the first efforts in this direction was described by Mairani et al. [123], presenting a MC treatment planning tool for proton therapy with PBS, including inverse optimization of single fields. An iterative optimization algorithm, running over a FLUKA MC calculated dose kernel, was used to optimize the beam weights. This approach was later extended to other ions. Plan optimization times were fairly large: several hours to optimize a multifield plan.

Shorter optimization times were obtained with frameworks that adopted GPU-based MC dose engines. Li et al. [181] developed an optimization code for proton therapy based on an adaptive particle sampling (APS) method to improve the efficiency of MC-based inverse optimization. Ma et al. [182] coupled a GPU-MC proton dose engine with a modified least-squares optimization method, achieving an optimization time of 30 min for a complex 3-field case.

2) Biological Effect-Based Optimization: In proton therapy optimization it is common to consider a constant RBE of 1.1 and the optimization process of the physical dose criteria is identical to RBE weighted dose criteria [177]. However, RBE is expected to vary along the particle path, because RBE varies with LET, as can be seen in Fig. 14. Here, the RBE_{10} (the RBE at 10% survival) is displayed as a function of LET for

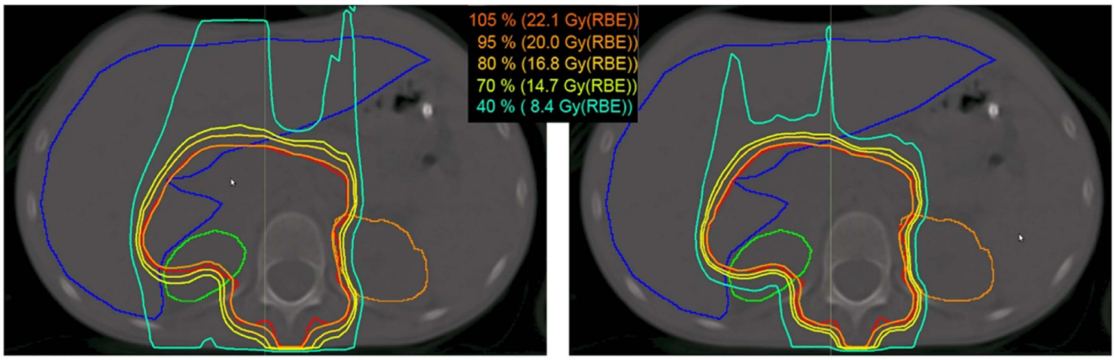

(a) (b)

Fig. 13. Isodose distributions for protons (left) and Helium atoms (right) of a neuroblastoma patient simulated with the FROG TPS, using two opposing beams from anterior and posterior direction. The differences in beam entrance and dose fall-off regions around the PTV between protons and helium ions are visible. The structures in red and blue are the PTV and the liver, respectively. The right and left kidney are highlighted by green and light brown contours, respectively. From [101], used under the creative commons attribution 4.0 license. (a) p^+. (b) ^{4}He.

TABLE I
VALUES FOR THE PERCENTAGE DOSE CONTRIBUTION OF PROTON, HELIUM, CARBON, AND OXYGEN BEAMS TO THE TARGET DOSE, OBTAINED FOR AN ORTHOGONAL-FIELD IMPACT PLANS WITH DIFFERENT PRESCRIBED VALUES OF LET, TO A CUBIC TARGET OF 8×8×8 CM^3 LOCATED AT THE CENTER OF THE WATER PHANTOM OF 20× 20× 20 CM^3. ADAPTED FROM INANIWA ET AL. [191]

Prescribed LET (keV/μm)	Percent dose contribution within target (%)			
	Proton	Helium	Carbon	Oxygen
7	57.0	39.3	2.3	1.4
50	12.9	13.2	30.5	43.4
72	4.1	3.5	12.0	80.4

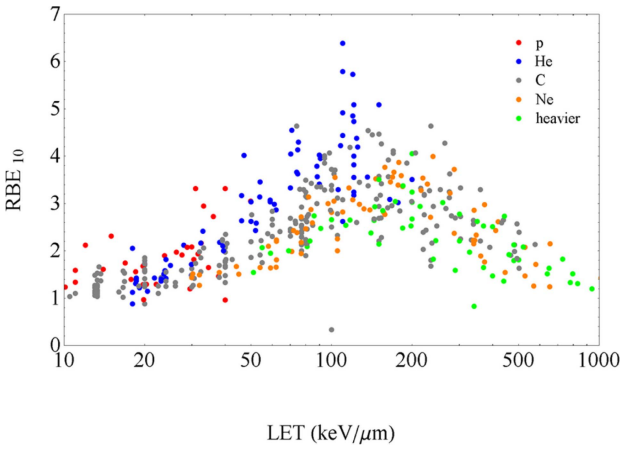

Fig. 14. Collection of data showing RBE_{10} versus LET for differentiation from published in vitro data. From [183], used under CC BY-NC-ND 4.0 DEED license.

various ions. In carbon therapy, RBE must be incorporated into the optimization.

In most clinically used TPSs, the RBE-weighted dose D_{RBE} (see Section IV-B) is optimized to satisfy requirements of target coverage and toxicity to OARs and healthy tissue. However, several TPSs have been developed that include other biological parameters into dose optimization.

Cao et al. [184] incorporated LET directly into the optimization of IMPT plans in their in-house developed TPS. The MatRad TPS [185] features the simultaneous optimization of RBE-weighted dose and nanometric ionization details [186]. The TRiP98 (Treatment Planning for Particles) tool [187], used clinically until 2008 during the carbon ion therapy pilot project and today for research, has since recently included new advanced optimization strategies, such as multiple field optimization, oxygen enhancement ratio (OER)-driven optimization, helium and oxygen beams characterization [188], multiple-ion (protons, helium, carbon, and oxygen) optimization [189], and volume effects [190]. Many advances have also been made at HIMAC, documented in a book by Kanematsu and Inaniwa [13]. Recently, an advanced TPS of intensity modulated particle therapy was developed, IMPACT (intensity modulated composite particle therapy) [191], which includes dose and LET optimization with multiple ion beams (protons, helium, carbon, oxygen). A prescription for dose and a dose-averaged LET value was given, which may depend on tumor type or size. Depending on the prescribed LET, the percentage dose contributions of proton, helium, carbon, and oxygen beams to the target dose vary, as illustrated in Table I. In particular, we can see that the percentage dose contribution of light ions is the highest when the prescribed LET is low, whereas the percentage dose contribution of oxygen is the highest when high LET is prescribed.

The above mentioned systems for biological dose optimization are based on analytical PB dose algorithms. Efforts have been made to merge MC dose engines into optimization platforms. Qin et al. [192] have developed a TPS for carbon therapy, based on the GPU MC dose engine goCMC code [134] mentioned in Section IV-C1. Advanced

TABLE II
SUMMARY OF POSSIBLE ERROR SOURCES IN PARTICLE THERAPY TREATMENTS

Patient related • Daily positioning and immobilization on couch • Internal organ motion • Inter-fractional anatomical changes: air cavities, tumor regression/growth, weight loss/gain, .. • Intra-fractional changes: cyclic (breathing, heart-beat), bladder, etc • Tumor related: staging, heterogenity, contours, ..
Physics related • CT Hounsfield Units: calibration • Conversion to stopping power • Dose calculation and treatment plan uncertainties: analytical algorithms, MC modeling, 3D patient description, ..
Others • Uncertainties on radiobiological models: RBE, .. • Imaging uncertainties: pre-treatment, in-room, in-vivo, .. • Machine delivery error sources: beam parameter errors (charge/monitoring unit, energy, etc), beam monitor, magnet settings, ..

radiobiological models together with an optimization module were adopted there to minimize the difference between the prescribed and actual biological effect. It achieved a total dose computation time, including spot simulation, optimization, and final dose calculation, of 10–40 min for clinical cases. The code was recently embedded in the commercial Varian Eclipse TPS. Finally, Tseung et al. [193] reported about a GPU-accelerated MC-based biological TPS for proton therapy, based on the fast GPU dose engine developed by Tseung et al. [131] (see Section IV-C1). This platform allows to take into account a variable RBE also for protons. It achieved a total computation time for a clinical plan of about 30 min.

VI. TREATMENT QUALITY VERIFICATION

It is well known that particle therapy dose distributions are sensitive to uncertainties [194], [195]. Various error sources are summarized in Table II. The dominant error sources are patient-related as well as radiobiological.

In the last decades, several advanced imaging and verification techniques have been developed to ensure an accurate dose delivery in particle therapy. They can be classified in pretreatment imaging techniques, imaging techniques during and right after delivery (including noninvasive monitoring techniques), and follow-up post-treatment imaging techniques.

Many of the pretreatment and follow-up imaging modalities are the same as those applied in conventional radiotherapy [196]. For instance, in the diagnostics and treatment planning phase, CT allows for an accurate knowledge about the target volume and position of organs-at-risk, and is essential for structure delineation and dose calculations. As mentioned in Section V-A, dual energy CT can improve the accuracy of particle therapy dose calculations [157], [197] and MRI can improve target definition [198], [199]. Also, positron-emission-tomography (PET) imaging can provide complementary information about the target in the diagnostic and treatment planning phase [200]. Proton radiography techniques are also used in the dose delivery phase. Various

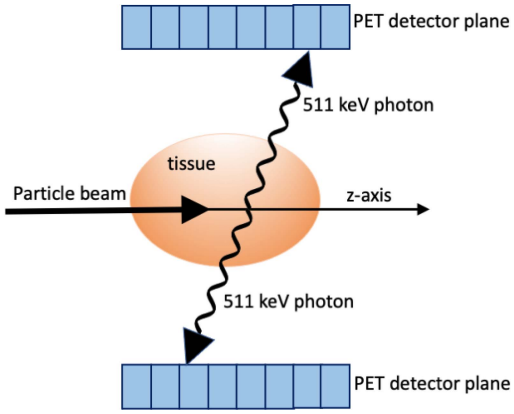

Fig. 15. Concept of treatment monitoring in particle therapy with PET imaging. Two coincidence photons with an energy of 511 keV are produced in the decay of a β^+-emitter, which can be detected with a PET system.

monitoring systems are available for in-room image guidance [3], [196], including kV and MV X-ray imaging-based methods, ultrasound, MRI, cone-beam CT (CBCT), Fan-Beam CT, and implantable dosimeters. Regarding treatment verification techniques, these are summarized in Section VI-A, focusing on verification techniques that were specifically developed for particle therapy dose delivery.

A. Noninvasive Nuclear Physics Imaging Methods

In conventional radiotherapy various techniques for in-vivo dosimetry exist, based on the beam transmission through the patient, reviewed for instance in [201]. Since particle therapy dose delivery is based on the stopping of the beams in the patient, such techniques cannot be used. Instead, nuclear interactions between the beam and the patient can be used to verify the treatment noninvasively. In fact, during the various stages of nuclear interactions [202], [203], different types of secondaries are produced, some of which exit the patient and can be detected. The idea to exploit nuclear reactions to estimate the beam range in tissue was first proposed by

Chatterjee at Berkeley in 1982 [204], who recognized that the β^+ emitting nuclei produced during irradiation with therapeutic particle beams could be measured with a PET detector to estimate the beam range. Techniques for in-vivo treatment verification by detection of nuclear fragments (also referred to as *in-vivo* range monitoring) are for instance described by Parodi [14] and Parodi and Polf [205]. The underlying physics and MC modeling are comprehensively described by Kraan [95]. Below we summarize and update some developments.

1) β^+ Emitting Isotopes: Among the many fragments produced in human tissue during irradiation are β^+ emitting fragments, including ^{15}O,^{11}C, ^{10}C, and ^{13}N (for a complete list see for instance [95]). Fig. 15 illustrates the concept of PET imaging in particle therapy.

Depending on the value of their half-life, the β^+ nuclei decays at a later time, emitting a positron, which after traveling a small distance (order of mm), annihilates with an electron in the medium into two coincidence gammas of 511 keV (in the positron-electron center of mass system). These can be measured with a PET detector and related to the delivered dose. In 1982 Chatterjee et al. [204] performed the first PET measurements and the first MC simulations of the PET signal arising from proton therapy were done by Del Guerra et al. [206], [207]. Since then, much research has been dedicated to range monitoring with PET, summarized for instance in various reviews [14], [95], [208], [209], [210]. Treatment verification can be done by day-to-day comparisons of the PET signal, or by comparing the detected PET signal with predictions from simulations. In the latter approach, initially analytical models were proposed [211], but later the MC approach was more widely applied [206], [210]. Recently, machine learning has been applied to reconstruct the dose in proton therapy from PET monitoring distributions [212].

The different PET data acquisition techniques would be offline and online PET. In the offline technique, data acquisition starts typically within 10 min after beam delivery outside the treatment room ("offline"), leading to a loss of signal due to decay of short-lived isotopes and physiological washout [213]. Other issues include co-registration problems and organ motion, making this technique generally considered less optimal [210]. Research and clinical applications are summarized in the above mentioned reviews.

In online techniques, data are acquired in the treatment room ("online"). where we can distinguish data acquisition during beam delivery ("in-beam") and data acquisition after beam delivery ("after-beam"). The advantage of data taking during dose delivery is that it allows to detect short-lived isotopes, that would otherwise remain undetected, and that the extracted information does not suffer from effects from wash-out, patient movements, etc. Most recent efforts in PET imaging are therefore ongoing in this direction.

Several dedicated in-beam PET systems were developed, all facing the challenge of making a PET system compatible with the beam delivery system. The most widely applied geometry for in-beam PET imaging is the planar geometry. This geometry was used in the first clinical application of in-beam PET for carbon therapy treatments at GSI in 2004 [214] and later also at the Kaswhiwa facility [215].

More recently, in Italy the DOPET dual head system [216] was developed, followed by an in-beam PET system in the context of the Innovative Solutions for Dosimetry in Hadrontherapy (INSIDE) [217] project. This system, displayed in Fig. 16, also features a secondary charged particle tracker (see Section VI-A3). The INSIDE PET detector has two planar PET heads that are spaced 60-cm apart, each with an active area of 10×25 cm^2 each. Lutetium fine silicate (LFS) is used as scintillating material, with $3.1 \times 3.1 \times 20$-mm^3 crystals and 3.2-mm pitch. The readout electronics consists of an array of Hamamatsu silicon photomultiplier (SiPM) coupled one-to-one to each crystal. The total field of view (FOV) is $11.2 \times 22.4 \times 26.4$ cm^3. The PET heads (together with the charged particle tracker) are mounted on a submillimetric precise mechanical cart. The system has completed the first phase of a clinical trial at CNAO with head-and-neck cases. The second phase is expected to start in 2024. Depending on the outcome, a decision will be taken about clinical implementation. Several data-analyses strategies have been explored, including voxel-based methods [218] and range evaluation methods [219], [220]. The latter are based on day-to-day data comparisons of PET data.

A dual head geometry was also used in studies investigating the feasibility to detect short-lived β^+ emitting isotopes during treatment, such as ^{12}N [221]. The main challenges here are the limited statistics and the adaptation to the typical beam structures of clinical accelerators. Another challenge is the capability of predicting nuclides with short lifetimes with MC simulations, because also the available experimental cross section data are scarce [10], [104], [222].

An in-beam PET system with particular shape has been developed for carbon therapy treatment monitoring [223]. The system has a cylindrical shape with 25-cm radius, cut by two parallel planes at a slant angle to form an open space (OPENPET) for the particle beam to pass through. Zr-doped GSO (GSOZ) scintillators were used, connected to position sensitive photomultiplier tubes. The spatial resolution was about 2.5 mm (FWHM).

Another novel geometrical arrangement for an in-beam scanner was recently proposed by Lovatti et al. [224], displayed in Fig. 17. Their design is based on 56 scintillator blocks of pixelated LYSO crystals, arranged in a pyramidal-step shape and distributed in spherical geometry with minimum gaps for maximum geometrical coverage. The main advantage of this geometry is that spherical-based shape has high performance in terms of spatial resolution and efficiency.

In Cracow a cost-effective PET technology, called Jagiellonian PET (J-PET), has been developed for a variety of applications, among which ion-therapy treatment monitoring [225]. Here, two scanner geometries were considered: 1) a double-layer full-ring geometry for an in-room imaging protocol and 2) a triple-layer dual-head geometry mounted in situ for in-beam PET monitoring. The system uses plastic scintillator strips, that are read out at both ends by SiPMs. Apart from standard PET imaging with coincidence photons, the system also allows for multiphoton imaging and positronium imaging.

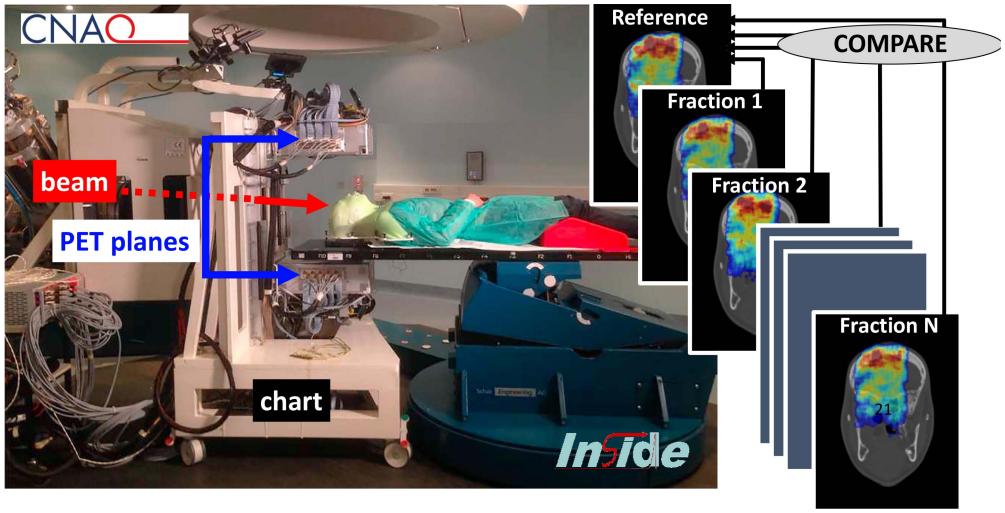

Fig. 16. PET monitoring system in the INSIDE system, installed at the CNAO particle therapy center in Pavia, Italy. The beam, PET planes, and mobile chart are indicated.

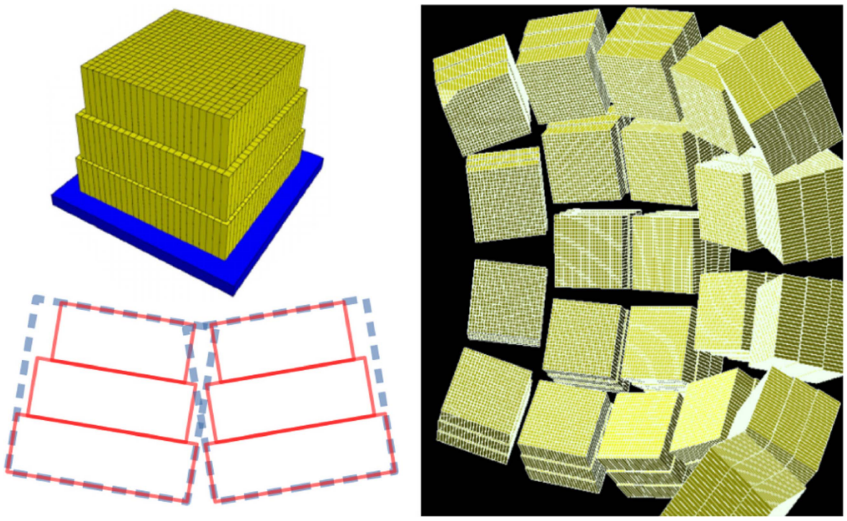

Fig. 17. Top Left: Single detector block, with the scintillator material (LYSO) in yellow and readout (SiPM) in blue. Bottom Left: Side display to show the step/pyramid configuration. Right: Scanner configuration. From [224], used under the CC BY 4.0 DEED license.

PET imaging in ^{12}C-ion therapy remains marginal, mostly due to the limited amount of β^+-emitters produced. These problems are overcome if β^+-radioactive ion beams are directly used for both treatment and imaging. Exploiting radioactive beams is the motivation of the biomedical applications of radioactive ion beams (BARB) experiment [226], that is currently ongoing at GSI in Darmstadt. The usage of an ^{11}C beam is expected to improve the count rate by an order of magnitude with respect to that of an ^{12}C beam, as is illustrated in Fig. 18. The main challenge is to obtain radioactive ion beams (^{11}C and ^{15}O) with sufficient intensity to treat tumors.

Finally, the usage of time-of-flight (TOF) PET [227] has been studied but not yet applied in clinical practise. This could help to improve the resolution of PET images, and for in-beam PET images it could reduce image artefacts.

2) Prompt Gammas: Along the particle path within a medium, nuclear reactions result in promptly emitted photons from the nuclear de-excitation phase of a nuclear reaction, with energies up to about 10 MeV. They are emitted isotropically from the mother nucleus and the distribution of PGs is correlated with the beam range. Since the original proposal in 2003 [228] and the proof of principle by Min et al. [229] for proton therapy treatment monitoring, much research was done. For comprehensive reviews please refer to recent works by Krimmer et al. [230] and Wrońska [231] and citations therein. The developed monitoring techniques exploit different characteristics of the emitted PGs, as sketched in Fig. 19.

1) *Position:* There is a strong correlation between the longitudinal PG profile and dose profile, making it possible to exploit PGs to retrieve the Bragg peak position. The most common approach to do this is with a collimated gamma camera. By placing the camera at 90° with respect to the beam-axis and moving the device parallel to the beam-axis, a 1-D PG profile can be measured (see Fig. 19(a). This was the design used in the first studies for proton [229] and carbon [232] irradiation and has since then been implemented by various research groups, leading to clinical applications.

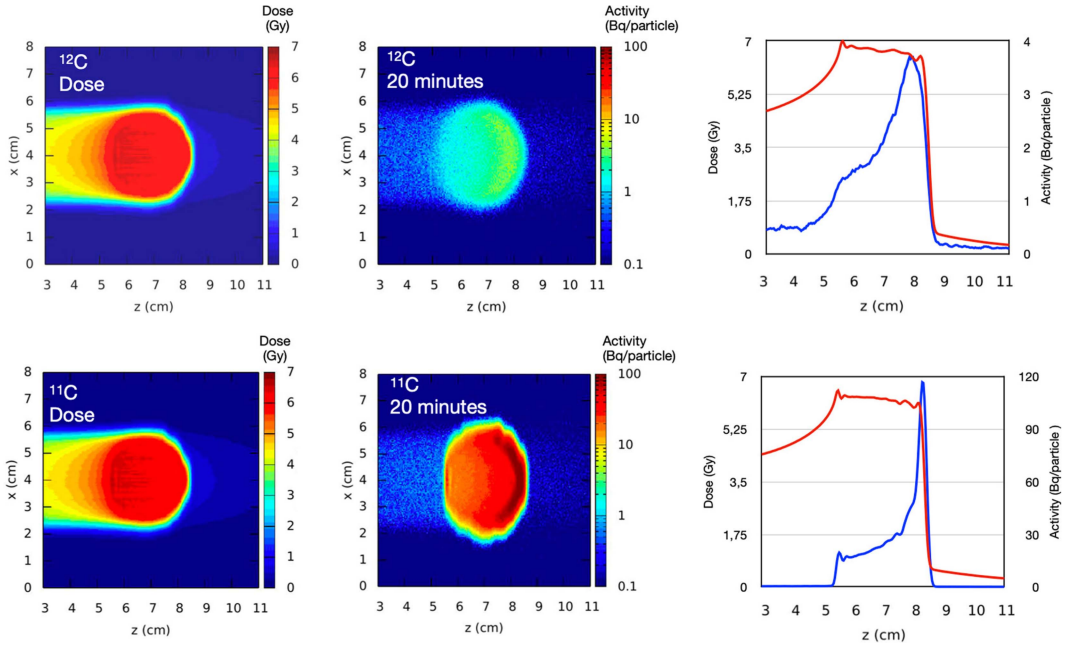

Fig. 18. Dose and PET distributions (20-min acquisition) obtained from a FLUKA MC simulation of a ^{12}C (top figures) and ^{11}C beam (bottom figures) stopping in a spherical water phantom. The left graphs show the 1-D distribution along z (beam-axis) of dose (red curve) and the activity (blue curve) distribution along the beam direction. From [226], used under the CC BY 4.0 DEED license.

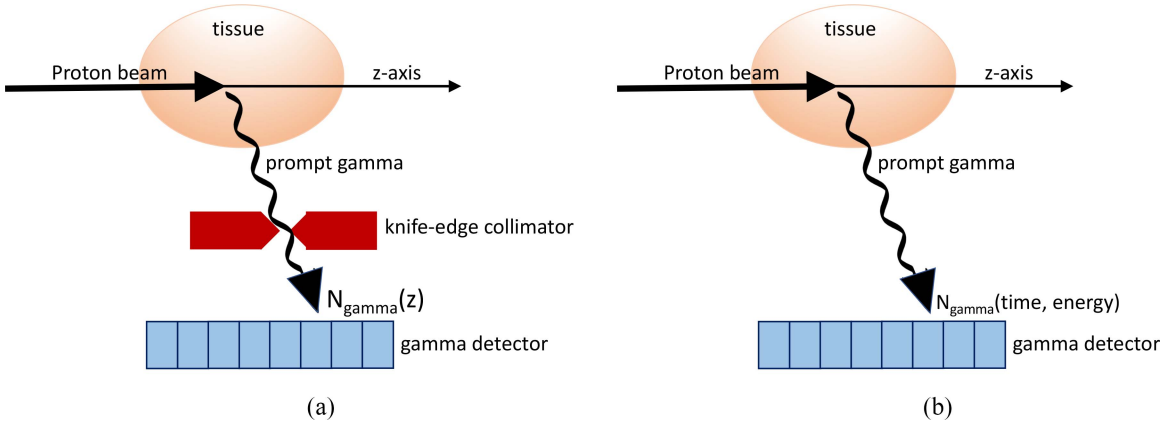

Fig. 19. Concept of PG imaging in particle therapy. (a) Knife-edge collimator design, allowing to measure the 1-D z-profile of the gamma to be measured. (b) Detection of energy or time of the emitted gammas.

A knife-edge shaped slit gamma camera prototype was used to measure the PG depth distribution during a (passive scattering) real proton treatment of a head and neck patient in Dresden in 2016 [233]. In this case a knife-edge shaped slit tungsten collimator projected the PG-ray emission profile produced by the particle beam in the patient onto an array of 40 individual scintillation detectors, arranged in two rows, resulting in a spatially resolved 1-D gamma profile. The analysis was focused on detecting interfractional variations. Variations of 2 mm were found in the PG profiles among the treatments, in accordance with the CT scans of the patient. A second prototype based on the same design was realized and tested clinically in Philadelphia for PBS proton treatments [234], where a 2-mm precision was obtained in detecting a range shift when combining several beams. Recently, in Dresden an improved version with better-position accuracy was used to investigate PG imaging for 5 patients with prostate cancer [235]. By comparing the 1-D PG emission profile detected during various treatment fractions with SP range predictions from an in-room DECT scan, the range prediction uncertainty of this device was estimated to be about 1 mm (2σ). The experimental setup is shown in Fig. 20. A version based on multiple slits was also recently built [236], where each slit is used to selectively detect the PGs that are emitted perpendicular to the proton beam. The advantage of such multislit designs is that the 1-D gamma profile can be measured without having to move the slit. Still based on collimation, pinhole cameras were developed for PG detection [237] but they have not yet been clinically applied. Besides collimator

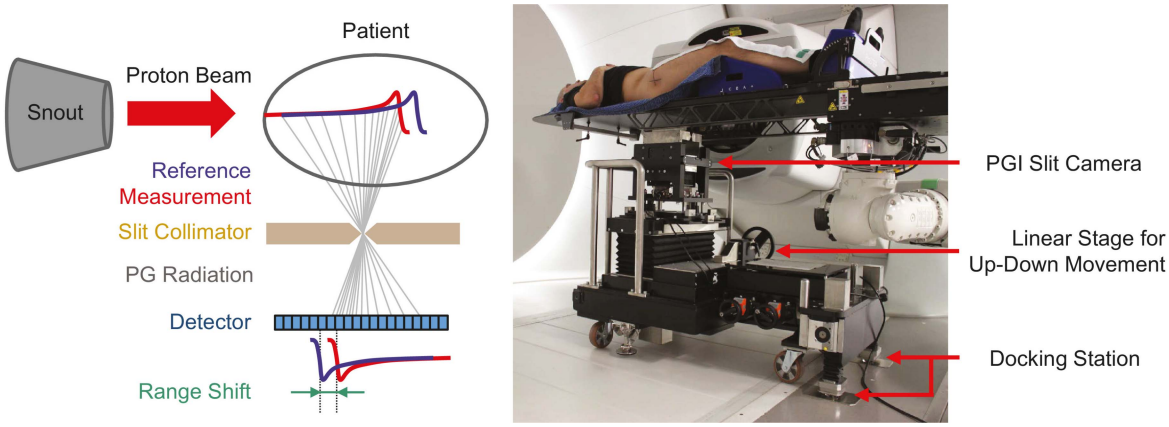

Fig. 20. Clinical implementation of the PG slit camera, with an illustration of the basic principle for PG imaging range verification with a slit (left) and the clinical setup for a patient irradiation at 90° gantry angle (right). Also visible is the docking and positioning system. From [235], used under the CC BY 4.0 DEED license.

designs, other configurations have been investigated, e.g., the Compton camera. In this setup, a multistage detector can measure the initial energy and direction of the photons undergoing Compton scattering in the detector. The ability of a prototype Compton camera to measure range shifts in water for PG rays emitted during delivery of clinical proton PBs was shown in [238]. A recent (preclinical) study is described by Muñoz et al. [239], where a multilayer Compton camera based on LaBr3 monolithic crystals and SiPMs (MACACO II Compton camera) together with a neural network for event reconstruction is used to measure 3-D-profiles and energy spectra. Images of the emission distribution at 4.4 MeV are reconstructed, allowing calculation of the distal fall-off and identification of target displacements of 3 mm.

2) *Energy detection*, as sketched in Fig. 19(b). The energy spectra of the prompt photons can be used as a tool to retrieve proton range and identify the traversed materials. In the nuclear reaction of the proton with a medium, a spectrum of PG rays is produced that is unique to the elemental composition of the medium. Proton range differences can be detected by comparing the measured PG energy spectrum with an a-priori estimation (for instance from MC simulations). The idea was originally proposed by Verburg and Seco [240] about a decade ago, and has recently evolved into a full-scale clinical prototype for proton range verification [241]. This detection system consists of eight $LaBr_3$:Ce scintillators and a tungsten collimator, mounted on a rotating frame. Energy- and time-resolved gamma-ray spectra during proton irradiation were measured at a clinical dose rate. A 1-mm precision was obtained for a phantom. PG spectroscopy was also recently proposed as an approach to monitor rectal radiation exposure in proton therapy [242].
3) *Time*, as sketched in Fig. 19(b). In time-resolved gamma imaging the idea is to exploit the correlation between the TOF spectra of PG emerging from a target with the energy of a particle beam. The technique was proposed for proton treatments in 2014 [243], [244]. Since the typical TOF is very short (typically a few hundred ps), it requires two detectors with excellent timing resolution. At present a prototype has been constructed close to clinical application, that makes use of fast scintillators [241]. Another novel technique that should exploit the TOF of PGs produced in proton therapy is PG time imaging (PGTI) [245]. They propose to measure the TOF between a beam monitor and a PG detector, and to use it to reconstruct the PG vertex distribution in 3-D with a noniterative reconstruction strategy. The experimental validation of the technique was recently published [246]. The PG emission time is also exploited in a study by Ferrero et al. [247], who show in a FLUKA MC feasibility study that the proton SP can be estimated by measuring the PG emission time along the whole proton path by using sophisticated time-dependent reconstruction techniques. Finally, Pennazio et al. [248] proposed to combine time and spatial information in a newly proposed method named spatio-temporal emission reconstruction PG timing (SER-PGT). A reconstruction method based on the numerical optimisation of a multidimensional likelihood function is proposed to directly reconstruct the prompt photon emission in the space and time inside the patient in proton therapy.

The main issues in PG imaging are the low-acquired statistics, the large background, and the integration into a clinical environment. Larger statistics is expected with radioactive beams [249] or by loading the tumor with label elements [250]. Regarding MC simulations, the complexity of nonelastic nuclear reactions makes it difficult to accurately predict and reproduce the level and shape of prompt γ emission spectra (see Section IV-A).

3) Charged Fragments: Another modality for treatment monitoring is interaction vertex imaging (IVI). It was proposed more than a decade ago by Amaldi et al. [251] for carbon ion-therapy range monitoring, and it has been investigated by different research groups [252], [253], [254]. The method is based on the detection of secondary charged particles, mostly protons, that exit the patient during particle irradiation, so as

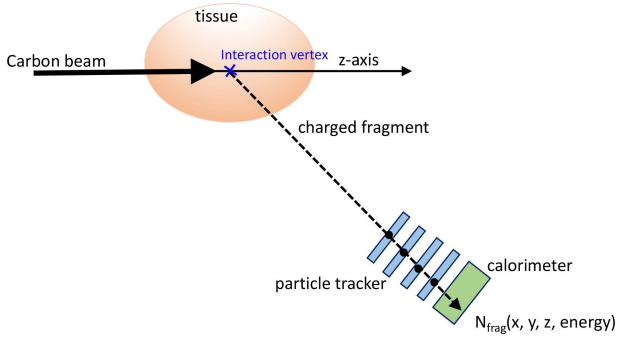

Fig. 21. Concept of IVI. The trajectories of the charged particles exiting from the irradiated material are reconstructed and extrapolated back to their production point.

to reconstruct back their nuclear emission vertex. The vertex position profile is correlated with the beam range (see Fig. 21) and delivered dose. Moreover, the production yield of the fragments along the beam path depends on the density and atomic mass of the crossed tissues. The detection of charged particles can be performed with a very high efficiency in an almost background-free environment.

Recently, this method has been tested for the first time for patients enrolled in a clinical trial carried out at CNAO in the context of the INSIDE project (see Section VI-A1), as described in [255]. The tracker is a multilayer scintillating fiber tracker. The spatial distributions of the emitted secondary fragments can be extracted at each treatment fraction, and the various fractions can be compared with each other to detect changes. The measured back-tracking resolution per fragment is about 7 mm at 50 cm from the patient [256]. A promising result by Fischetti et al. [255] is shown in Fig. 22, where the system was able to approximately localize the anatomical change, that was in this case located close to the beam entrance.

4) Neutral Fragments: Apart from charged fragments, neutral secondary particles, mostly neutrons, are emitted with energies ranging from a few MeV to hundred of MeV. From a dose-point of view, the importance of neutron production on dose is expected to be limited [257]. The technical challenges are the development of systems with high-detection efficiency for detecting neutrons with energies up to a few hundred MeV. A scintillator-based portable system was designed and tested to monitor neutrons produced in targets by therapeutic protons [258]. An organic scintillator (EJ-309) was used, that allowed effective discrimination between neutrons and photons using an offline charge-integration method. The detection of incident fast neutrons occurred here primarily through elastic scattering on hydrogen nuclei. Only neutrons with energies larger than a few hundred keV resulted in a detectable pulse. Finally, several feasibility studies have been performed regarding secondary neutron detection in particle therapy treatments [259], [260], but these have not yet been realized.

B. Proton Transmission Imaging

Particle range depends on the SP along the particle path and on the tissue composition. As mentioned in Section V-A, proton SP is derived from an x-ray-based CT scan, and the CT HUs are converted into particle SP with calibration curves, such as the commonly used Schneider calibration [155]. However, it can happen that tissues with the same HU have a different SP, and vice versa. This leads to uncertainties in range, that are typically accounted for by adding a margin around the tumor. Inaccuracies can be reduced if the protons themselves can be used for determining the SP. This is the concept of proton transmission imaging.

While in proton therapy, the protons stop in the vicinity of the tumor, in proton transmission imaging the protons pass through the patient and reach a detector. Thus, transmission requires the protons to have a higher-beam energy than that clinically needed for the therapy. A planar view can be made to obtain a proton radiograph (pR), where the source of image contrast is the energy loss of the transmitted protons (the integrated SPs of protons in the patient). By making many projections, a proton-CT (pCT) can be obtained. The usage of proton CT as pretreatment low-dose imaging technique is expected to reduce range uncertainties [261].

Detailed reviews about the history and physics of the proton CT are provided by Johnson et al. [262] and Poludniowski et al. [263]. Although the idea was originally proposed by Cormack in 1963 [264], it took up to 2004 until the first conceptual design for a pCT was presented by Schulte et al. [265]. The interest in proton radiography and proton CT has gradually grown. So far two experimental approaches have been adopted, based either on proton-integrating systems or on proton-tracking systems. The former approach is based on the energy deposition of a proton beam before and after the patient. The latter approach is based on the measurement of individual proton trajectories and energy deposition (proton tracking). Most instrumental efforts are currently based on proton-tracking systems [262], [266], an example of which is shown in Fig. 23.

Despite the technological efforts, the introduction into the clinic is slow. The main reason is the need for large-scale and expensive equipment to produce the required proton beams. The highest-proton energies needed for treatment are 230–250 MeV for protons, while 300–330 MeV is typically proposed for pCT. Reaching these higher energies implies the use of stronger magnets in the accelerator and beam transport, increasing the associated costs. Another limitation regards the image quality, which suffers from multiple scattering. The latter is reduced when using heavier ions than protons. However, reaching higher energies is even more complex in that case. Helium transmission imaging is for instance discussed in a recent work by Gehrke et al. [267]; carbon therapy transmission is discussed by Rinaldi et al. [268] and Magallanes et al. [269].

Finally, the irradiation of tissue by different ion types (for instance ^{12}C and ^{4}He), that are simultaneously accelerated and delivered, was recently explored with MC simulations [270], [271]. By adding a small fraction of helium to the primary carbon beam, it was shown that it is feasible to simultaneously irradiate the tumor with carbon ions to cure, and verify the patient thickness along the beam direction with helium ions through transmission imaging, thanks to the larger range of helium ions.

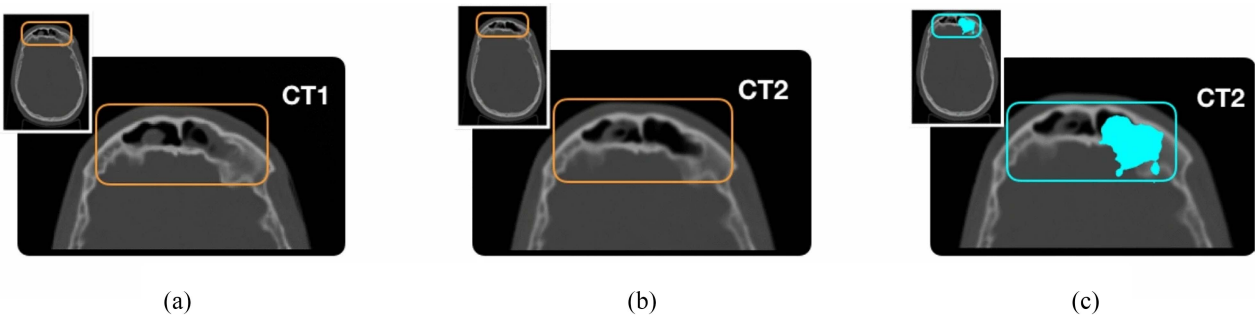

Fig. 22. Result of the INSIDE tracker data analysis. (a) Slice of the first CT of a patient. (b) Slice of the second CT of the same patient. In both images the region of the morphological change is highlighted in orange. (c) Second CT scan with superimposed in cyan the distribution of the points of closest approach, that were statistically incompatible between the first monitored fraction and the last one. From [255], used under the creative commons attribution 4.0 international license.

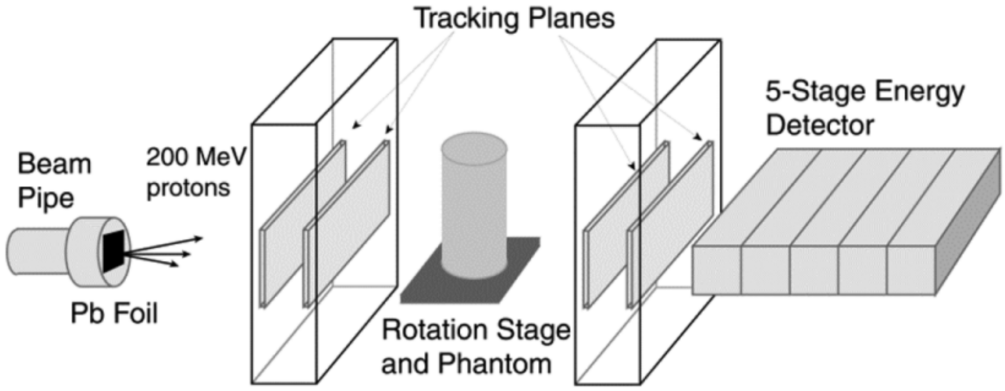

Fig. 23. Schematic layout of a typical pCT scanner designed to measure individual proton trajectories. Reproduced from [266].

VII. Future Developments

It is likely that in the next years superconducting magnet technologies will become the standard for accelerators and beam transport systems. Commercial vendors already offer superconducting cyclotrons, and next generation synchrotrons may be based on superconducting magnets. The development of ultralight iron-free accelerators is expected to reduce the size further. A more revolutionary technology is laser-driven accelerators [272], where electromagnetic energy from a laser pulse is transformed into kinetic energy of accelerated particles by letting laser pulses excite large-amplitude plasma density waves. Laser-driven accelerators are very compact and can produce beams with small width. However, important technical challenges remain to be faced before the beam characteristics are suitable for particle therapy, regarding intensity, particle energy spectrum, and pulse charge reproducibility. Other revolutionary techniques to make a particle therapy accelerator of the size of current X-ray systems, are: dielectric wall accelerators, dielectric wakefield accelerators, and plasma-based accelerators. However, all of them are far away from realization (see for instance [273]). To speed up technological innovations in accelerators and reduce the cost gap between particle therapy and conventional radiotherapy treatments, intense research in accelerator technology and science is needed. The available literature has evidenced the important role of specialized particle physics accelerator research centers, such as CERN in the development of new accelerator technologies [6], [19].

Technological developments in beam delivery techniques in both proton and carbon therapy have been focused on PBS, because of the advantages this technique offers as compared to passive scattering. Typically the dose is delivered from several beam directions with a (rotating) gantry, that covers a distance of several tens of meters. Gantries are large, heavy and complex systems, and much research is focused on the development of smaller and lighter gantries. It is expected that next generation gantries will be based on superconducting technologies. Due to the large size and high costs associated with gantries, the interest in gantry-free treatments is growing [73]. Although not all patients can be treated in this way, it could help to offer more affordable treatments and thus to increase the access to particle therapy worldwide.

There are several innovative beam delivery techniques that are gaining attention. There is clinical interest in arc therapy, where dose is delivered from many gantry angles. This technique can potentially offer improved target volume conformity and plan robustness, as shown for protons [274], [275] and carbon therapy [276]. The main technical challenge to be faced here is the realization of a fast rotating structure and how to deal with the increased complexity of treatment plan optimization algorithms. Another issue regarding dose delivery

is the usage of different particle types, that has been under study for a few years. From a treatment planning perspective, multi-ion treatment plans can lead to an advantageous LET distribution in the target and organs-at risk with respect to one type of ions [191], [276]. However from a technological perspective various important challenges associated with the simultaneous (or subsequent) delivery of different ions are still to be overcome, including switching ion source, beam currents, and so on. The clinical advantage of this modality would have to be confirmed with in-vitro studies. Charged particles can also be combined with photons, so that the advantages of both modalities can be exploited (see for example [277]).

Another dose delivery technique that has recently seen an explosion of interest is FLASH radiotherapy [278], which can be applied to particle therapy too. Here, the dose is delivered with ultrahigh dose rate ($>$ 40 Gy/s), allowing for a better sparing of healthy tissue with respect to conventional dose rates. For particle therapy, we can distinguish transmission FLASH, where the Bragg peak is located beyond the patient, and Bragg Peak FLASH, where the Bragg peak is located in the tumor region. The latter requires significantly more modifications to the beam line. FLASH is of great potential, but the exact radiobiological and chemical mechanisms are still unclear.

Another dose delivery approach is the usage of very small beams for dose delivery. Typical beam widths in PBS at isocenter range from 3 to 12 mm, but the usage of submillimetric particle beams has been proposed (mini-beams) [279]. This technique leads to more conformal plans and better sparing of OARs, especially the skin. Existing beam transport and delivery systems are not designed to deliver submillimetric beams, and most experiments so far have relied on mechanical collimation. New focusing techniques with solenoid and quadrupole magnets as well as plasma lenses are being investigated. Finally, although not directly connected to charged particle therapy, a future technology that is worth mentioning is boron neutron capture therapy, a radiation therapy that relies on the use of external high-intensity epithermal (energy 0.5 to 10 keV) neutrons for the generation of energetic alpha particles ($^{10}\mathrm{B} + \mathrm{n} \rightarrow {}^{7}\mathrm{Li} + {}^{4}\mathrm{He}$) to destroy cells within the tumor [280]. Originally proposed in the 1930s, it recently gained renewed interest thanks to the technological breakthrough made in compact accelerator-based production of neutrons, compared to the earlier used research reactors.

Much research in particle therapy make use of MC simulations, ranging from hardware design studies to dose calculations and treatment monitoring [194]. Hadronic models are in continuous development and new future data are expected to increase their accuracy [10]. Increasing the speed of MC simulations is a key priority [127], [134], and more developments aimed at accelerating MC calculations are expected. To facilitate running computationally expensive MC simulations, access to powerful computational resources, such as open-source Web-based cloud computing environments, could be a solution if in-house resources are not sufficient.

Regarding treatment planning calculations, the literature research conducted for this review demonstrates that the clinical interest in fast (GPU or other techniques) MC-based treatment plan calculations has exploded in the last decade. Several commercial TPSs now offer the option of MC dose (forward) calculations as independent calculation. On the other hand, the usage of MC in inverse dose calculations is still limited to research, but the evolution in computer speed and available memory may change it. Regarding radiobiological treatment planning, precise calculations of biological dose remain a key challenge. With different biological models in use in different parts of the world, there are substantial uncertainties in the calculation of RBE [8]. Worldwide collaboration between research groups of different facilities is essential to reduce such uncertainties.

More advanced dose delivery techniques require more accurate imaging and treatment verification techniques. Certainly real-time MRI-based online adaptation is of great interest, but still face significant challenges when applied to particle therapy, such as the mutual electromagnetic interactions, between beam and MRI field [198]. In-vivo noninvasive imaging techniques should be used as an additional guarantee that a plan is delivered correctly. Verification strategies that allow for a real-time response, such as in-beam PET or PGs, are particularly appealing [210]. Combining different modalities is also of great interest (see [217] and [281]). A fundamentally different technique for in-vivo range verification in proton therapy is acoustic imaging, aimed at the detection of proton-induced radio-frequency signal [282], [283]. Research started about a decade ago and recently 3-D dosimetry was achieved with the help of deep learning methods [284].

There are many other topics that would deserve attention, such as hypofractionation, 4-D planning, radiobiological topics, biomathematical modeling of radiation response, integration with systemic therapies, including immunotherapy and innovative imaging techniques, such as Cherenkov, photophosrescence, positronium imaging, etc. However, these are either discussed in a different research context, or too far away from clinical application. It was therefore outside the scope of the current work to discuss them.

VIII. Conclusion

The past decades have witnessed significant developments of technologies in the field of particle therapy. Research was driven by the necessity to improve treatment quality as well as to reduce costs. In this review we have described several important technological advancements in proton and carbon therapy, that are now integrated into routine clinical practice or are near to be used in clinical facilities. The topics discussed here regarded both hardware and software developments, ranging from particle accelerators and beam transport to MC simulations, treatment planning and verification techniques. To guide the reader through the rapidly evolving physical, technological and clinical research in particle therapy, an extended and detailed list of references has been included.

ACKNOWLEDGMENT

The authors thank doctor V. Vitolo for providing us with Fig. 1. The authors thank H. Paganetti for providing us with Fig. 10. The authors thank A. Ferrari for providing us with the data for Fig. 9. The authors declare that they have no known conflicts of interest in terms of competing financial interests or personal relationships that could have an influence or are relevant to the work reported in this article.

REFERENCES

[1] M. Tambas et al., "Current practice in proton therapy delivery in adult cancer patients across Europe," *Radiother. Oncol.*, vol. 167, no. 12, pp. 7–13, 2021.

[2] J. S. Loeffler and M. Durante, "Charged particle therapy—Optimization, challenges and future directions," *Nat. Rev. Clin. Oncol.*, vol. 10, no. 5, pp. 411–424, 2013.

[3] M. Vidal, C. Moignier, A. Patriarca, M. Sotiropoulos, T. Schneider, and L. De Marzi, "Future technological developments in proton therapy—A predicted technological breakthrough," *Cancer/Radiotherapy*, vol. 25, nos. 6–7, pp. 554–564, 2021.

[4] E. W. Collings, L. Lu, N. Gupta, and M. D. Sumption, "Accelerators, gantries, magnets and imaging systems for particle beam therapy: Recent status and prospects for improvement," *Front. Oncol.*, vol. 11, Feb. 2022, Art. no. 737837.

[5] J. Yap, A. De Franco, and S. Sheehy, "Future developments in charged particle therapy: Improving beam delivery for efficiency and efficacy," *Front. Oncol.*, vol. 11, no. 12, 2021, Art. no. 780025.

[6] S. Myers, A. Degiovanni, and J. Farr, "Future prospects for particle therapy accelerators," *Rev. Accelerator Sci. Technol.*, vol. 10, no. 8, pp. 49–92, 2019.

[7] M. Durante, J. Debus, and J. Loeffler, "Physics and biomedical challenges of cancer therapy with accelerated heavy ions," *Nat. Rev. Phys.*, vol. 3, no. 9, pp. 1–14, 2021.

[8] W. Tinganelli and M. Durante, "Carbon ion radiobiology," *Cancers*, vol. 12, no. 10, p. 3022, 2020.

[9] M. Scholz, "State-of-the-art and future prospects of ion beam therapy: Physical and biological aspects," *IEEE Trans. Radiat. Plasma Med. Sci.*, vol. 4, no. 2, pp. 147–160, Mar. 2020.

[10] S. Muraro, G. Battistoni, and A. C. Kraan, "Challenges in MC simulations as clinical and research tool in particle therapy: A review," *Front. Phys.*, vol. 8, Nov. 2020, Art. no. 567800.

[11] J. Seco and F. Verhaegen, *MC Techniques in Radiation Therapy*. Boca Raton, FL, USA: CRC Press, 2013.

[12] H. Nystrom, M. F. Jensen, and P. W. Nystrom, "Treatment planning for proton therapy: What is needed in the next 10 years?" *Brit. J. Radiol.*, vol. 93, no. 7, 2019, Art. no. 20190304.

[13] N. Kanematsu and T. Inaniwa, "Treatment planning of carbon–ION radiotherapy," in *Carbon-LON Radiotherapy: Principles, Practices, and Treatment Planning*, H. Tsujii, T. Kamada, T. Shirai, K. Noda, H. Tsuji, and K. Karasawa, Eds. Tokyo, Japan, Springer, 2014, ch. , pp. 87–97.

[14] K. Parodi, "Latest developments in *in-vivo* imaging for proton therapy," *Brit. J. Radiol.*, vol. 93, no. 12, 2019, Art. no. 20190787.

[15] H. Peng et al., "Recent advancements of artificial intelligence in particle therapy," *IEEE Trans. Radiat. Plasma Med. Sci.*, vol. 7, no. 3, pp. 213–224, Mar. 2023.

[16] R. Mohan, "A review of proton therapy—Current status and future directions," *Precis. Radiat. Oncol.*, vol. 6, pp. 164–176, May 2022.

[17] C. Graeff, L. Volz, and M. Durante, "Emerging technologies for cancer therapy using accelerated particles," *Progr. Nucl. Phys.*, vol. 131, Jul. 2023, Art. no. 104046.

[18] M. J. Schippers. "Cyclotrons for particle therapy." 2017. [Online]. Available: https://cds.cern.ch/record/2315176/files/1804.08541.pdf

[19] E. Benedetto et al. "Comparison of accelerator designs for an ion therapy and research facility." 2020. [Online]. Available: https://cds.cern.ch/record/2748083?ln=en

[20] J. H. Lawrence, "Proton irradiation of the pituitary," *Cancers*, vol. 10, no. 4, pp. 795–798, 1957.

[21] "Particle Therapy Co-Operative Group." 2024. [Online]. Available: https://www.ptcog.ch/

[22] Y. Jongen et al., "Progress report on the IBA-SHI small cyclotron for cancer therapy," *Nucl. Instrum. Meth. Phys. Res. B*, vol. 79, no. 1, pp. 885–89, 1993.

[23] M. Schillo et al., "Compact superconducting 250-MeV proton cyclotron for the PSI proscan proton therapy project," *AIP Conf. Proc.*, vol. 600, no. 12, pp. 37–39, 2001.

[24] J. Yoshida et al. "Excitation test of superconducting magnet in a 230-MeV isochronous cyclotron for proton therapy," *IEEE Trans. Appl. Supercond.*, vol. 30, no. 4, pp. 1–5, Jun. 2020.

[25] H. W. Kim, J. Kang, B. H. Hong, and I. S. Jung, "Design study of the KIRAMS-430 superconducting cyclotron magnet," *Nucl. Instrum. Methods Phys. Res. A, Accelerators, Spectrometers, Detectors Assoc. Equip.*, vol. 823, pp. 26–31, Jul. 2016.

[26] Y. Jongen et al., "Compact superconducting cyclotron c400 for hadron therapy," *Nucl. Instrum. Methods Phys. Res. A, Accelerators, Spectrometers, Detectors Assoc. Equip.*, vol. 624, no. 12, pp. 47–53, 2010.

[27] V. Smirnov and S. Vorozhtsov, "Feasibility study of a cyclotron complex for hadron therapy," *Nucl. Instrum. Methods Phys. Res. A, Accelerators, Spectrometers, Detectors Assoc. Equip.*, vol. 887, pp. 114–121, Apr. 2018.

[28] A. Radovinsky et al., "Superconducting magnets for ultra light and magnetically shielded, compact cyclotrons for medical, scientific, and security applications," *IEEE Trans. Appl. Supercond.*, vol. 24, no. 3, pp. 1–5, Jun. 2014.

[29] A. M. Koehler and K. Johnson, "Clinical 'experience with the 160-MeV proton beam and some implications for designers,'" *IEEE Trans. Nucl. Sci.*, vol. NS-26, no. 2, pp. 2253–56, Apr. 1979.

[30] T. Zhao et al., "Commissioning and initial experience with the first clinical gantry-mounted proton therapy system," *J. Appl. Clin. Med. Phys.*, vol. 17, no. 2, pp. 24–40, 2016.

[31] R. Pidikiti et al., "Commissioning of the world's first compact pencil-beam scanning proton therapy system," *J. Appl. Clin. Med. Phys.*, vol. 19, no. 11, pp. 94–105, 2017.

[32] J. R. Castro et al., "Treatment of cancer with heavy charged particles," *Int. J. Radiat. Oncol. Biol. Phys.*, vol. 8, no. 12, pp. 2191–2198, 1982.

[33] J. Slater, "Development and operation of the LOMA LINDA university medical center proton facility," *Technol. Cancer Res. Treatment*, vol. 6, no. 9, pp. 67–72, 2007.

[34] *Decommissioning of Particle Accelerators*, Int. Atomic Energy Agency, Vienna, Austria, 2020.

[35] O. Mohamad, H. Makishima, and T. Kamada, "Evolution of carbon ion radiotherapy at the National institute of radiological sciences in Japan," *Cancers*, vol. 10, no. 3, p. 66, 2018.

[36] S. Rossi, "Hadron therapy achievements and challenges: The CNAO experience," *Physics*, vol. 4, no. 1, pp. 229–257, 2022.

[37] U. Amaldi et al., "The hadron therapy project," *Radiol. Med.*, vol. 86, no. 5, pp. 669–679, 1993.

[38] M. G. Pullia et al., "Explorative studies of an innovative superconducting gantry," *J. Phys. Conf.*, vol. 2420, Jun. 2023, Art. no. 12099.

[39] Y. Iwata, T. Shirai, and K. Mizushima, "Design of a compact superconducting accelerator for advanced heavy-ion therapy," *Nucl. Instrum. Methods Phys. Res. A, Accelerators, Spectrometers, Detectors Assoc. Equip.*, vol. 1053, Aug. 2023, Art. no. 168312.

[40] C. Cuccagna et al., "Beam characterization for the TULIP accelerator for protontherapy through full Monte Carlo simulations," *Eur. J. Med. Phys.*, vol. 42, no. S1, p. 11, 2017.

[41] Y. Iwata et al. "Multiple-energy operation with extended flattops at HIMAC," *Nucl. Instrum. Methods Phys. Res. A, Accelerators, Spectrometers, Detectors Assoc. Equip.*, vol. 624, no. 1, pp. 33–38, 2010.

[42] A. Degiovanni et al., "Linac booster for high energy proton therapy and imaging," *Phys. Rev. Accel. Beams*, vol. 21, no. 6, 2018, Art. no. 64701.

[43] K. Peach et al., "Conceptual design of a nonscaling fixed field alternating gradient accelerator for protons and carbon ions for charged particle therapy," *Phys. Rev. Accel. Beams*, vol. 16, no. 3, 2013, Art. no. 30101.

[44] S. L. Sheehy et al., "Characterization techniques for fixed-field alternating gradient accelerators and beam studies using the KURRI 150-MeV proton FFAG," *Progr. Theor. Exp. Phys.*, vol. 7, no. 7, 2016, Art. no. 73G01.

[45] J. Son et al., "Development of optical fiber based measurement system for the verification of entrance dose map in pencil beam scanning proton beam," *Sensors*, vol. 18, no. 1, p. 227, 2018.

[46] H. Chen, W. Matysiak, S. Flampouri, R. Slopsema, and Z. Li, "Dosimetric evaluation of hybrid brass/stainless-steel apertures for proton therapy," *Phys. Med. Biol.*, vol. 59, no. 8, pp. 5043–5060, 2014.

[47] V. Moskvin, C. Cheng, M. McDonald, and I. Das, "Reduced secondary neutrons and occupational exposure with optimization of beam shaping device material in proton therapy," *Int. J. Radiat. Oncol. Biol. Phys.*, vol. 87, no. 10, pp. S185–S186, 2013.

[48] S. B. Jia et al., "Designing a range modulator wheel to spread-out the Bragg peak for a passive proton therapy facility," *Nucl. Instrum. Methods Phys. Res. A, Accelerators, Spectrometers, Detectors Assoc. Equip.*, vol. 806, no. 10, pp. 101–108, 2015.

[49] E. Pedroni et al., "The 200-MeV proton therapy project at the Paul Scherrer Institute: Conceptual design and practical realization," *Med. Phys.*, vol. 22, no. 1, pp. 37–53, 1995.

[50] T. Furukawa et al., "Development of fast scanning magnets and their power supply for particle therapy," *IEEE Trans. Appl. Supercond.*, vol. 24, no. 3, pp. 1–4, Jun. 2014.

[51] M. Mishra et al., "Proton beam therapy delivered using pencil beam scanning vs. Passive scattering/uniform scanning for localized prostate cancer: Comparative toxicity analysis of PCG 001-09," *Clin. Transl. Radiat. Oncol.*, vol. 19, no. 8, pp. 80–86, 2019.

[52] V. Maradia et al., "Ultra-fast pencil beam scanning proton therapy for locally advanced non-small-cell lung cancers: Field delivery within a single breath-hold," *Radiother. Oncol.*, vol. 174, pp. 23–29, Sep. 2022.

[53] L. Zhao et al., "Developing an accurate model of spot-scanning treatment delivery time and sequence for a compact superconducting synchrocyclotron proton therapy system," *Radiat. Oncol.*, vol. 17, no. 5, p. 87, 2022.

[54] Z. Mei et al., "Optimization of a B4C/graphite composite energy degrader and its shielding for a proton therapy facility," *Nucl. Instrum. Methods Phys. Res. A, Accelerators, Spectrometers, Detectors Assoc. Equip.*, vol. 995, no. 2, 2021, Art. no. 165127.

[55] E. Oponowicz, H. L. Owen, S. Psoroulas, and D. Meer, "Geometry optimisation of graphite energy degrader for proton therapy," *Eur. J. Med. Phys.*, vol. 76, no. 8, pp. 227–235, 2020.

[56] V. Maradia et al., "A new emittance selection system to maximize beam transmission for low-energy beams in cyclotron-based proton therapy facilities with gantry," *Med. Phys.*, vol. 48, no. 12, pp. 7613–22, 2021.

[57] M. Goethem, R. Meer, H. Reist, and J. Schippers, "GEANT4 simulations of proton beam transport through a carbon or beryllium degrader and following a beam line," *Phys. Med. Biol.*, vol. 54, no. 10, pp. 5831–46, 2009.

[58] V. Maradia, D. Meer, R. Dölling, D. C. Weber, A. J. Lomax, and S. Psoroulas, "Demonstration of momentum cooling to enhance the potential of cancer treatment with proton therapy," *Nat. Phys.*, vol. 19, pp. 1437–1444, Jul. 2023.

[59] D. Mah et al., "Retrospective analysis of reduced energy switching and room switching times on throughput efficiency of a multi-room proton therapy center," *Brit. J. Radiol.*, vol. 93, no. 1107, 2020, Art. no. 20190820.

[60] T. F. Delaney and H. M. Kooy, *Proton and Charged Particle Radiotherapy*. Philadelphia, PA, USA: Lippincott Williams and Wilkins, 2008.

[61] O. J$^{\acute{}}$ akel, G. Kraft, and C. Karger, "The history of ion beam therapy in Germany," *Zeitschrift fur Medizinische Physik*, vol. 32, no. 1, pp. 6–22, 2022.

[62] A. Gerbershagen, C. Calzolaio, D. Meer, S. Sanfilippo, and M. Schippers, "The advantages and challenges of superconducting magnets in particle therapy," *Supercond. Sci. Technol.*, vol. 29, no. 8, 2016, Art. no. 83001.

[63] J. Alonso and T. Antaya, "Superconductivity in medicine" *Rev. Accelerator Sci. Technol.*, vol. 5, no. 1, pp. 227–263, 2012.

[64] K. P. Nesteruk, C. Calzolaio, D. Meer, V. Rizzoglio, M. Seidel, and J. M. Schippers, "Large energy acceptance gantry for proton therapy utilizing superconducting technology," *Phys. Med. Biol.*, vol. 64, no. 7, 2019, Art. no. 175007.

[65] Y. Iwata et al., "Beam commissioning of a superconducting rotating-gantry for carbon-ion radiotherapy," *Nucl. Instrum. Methods Phys. Res. A, Accelerators, Spectrometers, Detectors Assoc. Equip.*, vol. 834, no. 7, pp. 71–80, Oct. 2016.

[66] S. Takayama et al., "Design and magnetic field measurement of the superconducting magnets for the next-generation rotating gantry," *IEEE Trans. Appl. Supercond.*, vol. 32, no. 6, pp. 1–4, Sep. 2022.

[67] Y. Iwata, T. Shirai, and K. Noda, "Design of superconducting magnets for a compact carbon gantry," *IEEE Trans. Appl. Supercond.*, vol. 26, no. 4, pp. 1–4, Jun. 2016.

[68] S. Takayama et al., "Design and test results of superconducting magnet for heavy-ion rotating gantry," *J. Phys. Conf.*, vol. 871, no. 7, 2017, Art. no. 12083, doi: 10.1088/1742-6596/871/1/012083.

[69] D. Meyer and R. Flasck, "A new configuration for a dipole magnet for use in high energy physics applications," *Nucl. Instrum. Meth. Phys. Res.*, vol. 80, no. 2, pp. 339–341, 1970.

[70] L. Brouwer et al., "Design of an achromatic superconducting magnet for a proton therapy gantry," *IEEE Trans. Appl. Supercond.*, vol. 27, no. 4, pp. 1–6, 2017, doi: 10.1109/TASC.2016.2628305.

[71] L. Piacentini et al., "Comparative study on scenarios for rotating gantry mechanical structures" *Open Res. Eur.*, vol. 2, no. 5, p. 55, 2022.

[72] E. Felcini, L. Bottura, J. van Nugteren, G. de Rijk, G. Kirby, and B. Dutoit, "Magnetic design of a superconducting toroidal gantry for hadron therapy," *IEEE Trans. Appl. Supercond.*, vol. 30, no. 4, pp. 1–5, Jun. 2020.

[73] N. Schreuder, X. Ding, and Z. Li, "Fixed beamlines can replace gantries for particle therapy," *Med. Phys.*, vol. 49, no. 4, pp. 2097–2100, 2022.

[74] S. Yan, H.-M. Lu, J. Flanz, J. Adams, A. Trofimov, and T. Bortfeld, "Reassessment of the necessity of the proton gantry: Analysis of beam orientations from 4332 treatments at the Massachusetts General Hospital proton center over the past 10 years," *Int. J. Radiat. Oncol. Biol. Phys.*, vol. 95, no. 9, pp. 224–233, 2015.

[75] L. Volz, Y. Sheng, M. Durante, and C. Graeff, "Considerations for upright particle therapy patient positioning and associated image guidance," *Front. Oncol.*, vol. 12, Jul. 2022, Art. no. 930850.

[76] X. Li et al. "The first prototype of spot-scanning proton arc treatment delivery," *Radiother. Oncol.*, vol. 137, no. 8, pp. 130–136, 2019.

[77] X. Zhang et al., "Development of an isocentric rotating chair positioner to treat patients of head and neck cancer at upright seated position with multiple non-planar fields in a fixed carbon-ion beamline," *Med. Phys.*, vol. 47, no. 6, pp. 2450–2460, 2020.

[78] Y. Sheng et al., "Performance of a 6D treatment chair for patient positioning in an upright posture for fixed ion beam lines," *Front. Oncol.*, vol. 10, no. 2, p. 122, 2020.

[79] J. Sun et al., "Clinical implementation of a 6d treatment chair for fixed ion beam lines," *Front. Oncol.*, vol. 11, no. 6, 2021, Art. no. 694749.

[80] V. Patera and A. Sarti, "Recent advances in detector technologies for particle therapy beam monitoring and dosimetry," *IEEE Trans. Radiat. Plasma Med. Sci.*, vol. 4, no. 2, pp. 133–146, Mar. 2020.

[81] A. Colautti et al., "Therapeutic proton beams: LET, RBE and micro-dosimetric spectra with gas and silicon detectors," *Radiat. Meas.*, vol. 136, Aug. 2020, Art. no. 106386.

[82] S. Agostinelli et al., "GEANT4—A simulation toolkit," *Nucl. Instrum. Methods Phys. Res. A, Accelerators, Spectrometers, Detectors Assoc. Equip.*, vol. 506, no. 3, p. 1368, 2003.

[83] T. T. Böhlen et al., "The FLUKA code: Developments and challenges for high energy and medical applications," *Nucl. Data Sheets*, vol. 120, no. 6, pp. 211–214, 2014.

[84] G. Battistoni et al., "The FLUKA code: An accurate simulation tool for particle therapy," *Front. Oncol.*, vol. 6, p. 116, May 2016.

[85] M. E. Rising et al., "MCNP code version 6.3.0 release notes," Los Alamos Nat. Lab., Los Alamos, NM, USA, Rep. LA-UR-22-33103, Jan. 2023.

[86] N. Bassler, D. Hansen, A. Lühr, B. Thomsen, J. B. Petersen, and N. Sobolevsky, "SHIELD-HIT12A—A MC particle transport program for ion therapy research," *J. Phys. Conf.*, vol. 489, no. 2, 2014, Art. no. 12004.

[87] T. Sato et al., "Features of particle and heavy ion transport code system (PHITS) version 3.02," *J. Nucl. Sci. Technol.*, vol. 55, no. 1, pp. 1–7, 2018.

[88] J. F. Ziegler, M. D. Ziegler, and J. P. Biersack, "SRIM—The stopping and range of ions in matter (2010)," *Nucl. Instrum. Meth. Phys. Res. B*, vol. 268, nos. 11–12, pp. 1818–1823, 2010.

[89] B. Faddegon et al., "The TOPAS tool for particle simulation, a MC simulation tool for physics, biology and clinical research," *Phys. Med.*, vol. 72, p. 114, Apr. 2020.

[90] T. Aso et al., "GEANT4 based simulation framework for particle therapy system," in *Proc. IEEE Nucl. Sci. Symp. Conf. Rec.*, 2007, pp. 1–8.

[91] S. Jan et al., "GATE V6: A major enhancement of the GATE simulation platform enabling modelling of CT and radiotherapy," *Phys. Med. Biol.*, vol. 56, no. 4, p. 881, 2011.

[92] L. J. Nevay et al., "BDSIM: An accelerator tracking code with particle-matter interactions," *Comput. Phys. Commun.*, vol. 252, Jul. 2020, Art. no. 107200.

[93] R. L. Workman et al., "The review of particle physics as of 2020," *Prog. Theor. Exp. Phys*, vol. 2022, no. 8, 2022, Art. no. 083C01.

[94] M. Durante and H. Paganetti, "Nuclear physics in particle therapy: A review," *Rep. Progr. Phys.*, vol. 79, no. 9, 2016, Art. no. 96702.

[95] A. C. Kraan, "Range verification methods in particle therapy: Underlying physics and MC modeling," *Front. Oncol.*, vol. 5, p. 150, Jul. 2015.

[96] D. J. Buglewicz et al., "Biological effects of monoenergetic carbon ions and their associated secondary particles," *Front. Oncol.*, vol. 12, Feb. 2022, Art. no. 788293.

[97] A. Mirandola et al., "Dosimetric commissioning and quality assurance of scanned ion beams at the Italian National Center for oncological hadrontherapy," *Med. Phys.*, vol. 42, no. 9, p. 528, 2015.

[98] P. Arce et al., "Report on G4-MED, a GEANT4 benchmarking system for medical physics applications developed by the GEANT4 medical simulation benchmarking group," *Med. Phys.*, vol. 48, no. 5, pp. 19–56, 2020.

[99] T. Tessonnier et al., "Dosimetric verification in water of a MC treatment planning tool for proton, helium, carbon and oxygen ion beams at the Heidelberg ion beam therapy center," *Phys. Med. Biol.*, vol. 62, no. 16, p. 6579, 2017.

[100] F. Horst et al., "Measurements of ^{4}He charge and mass changing cross sections on H,C,O, and Si targets in the energy range 70–220 MeV/u for radiation transport calculations in ion-beam therapy," *Phys. Rev. C*, vol. 99, Jan. 2019, Art. no. 14603. [Online]. Available: https://doi.org/10.1103/PhysRevC.99.014603

[101] A. Mairani et al., "Roadmap: helium ion therapy," *Phys. Med. Biol.*, vol. 67, no. 4, 2022, Art. no. 15TR02.

[102] T. Akagi et al., "Experimental study for the production cross section of positron emitters induced from 12C and 16O nuclei by low-energy proton beams," *Radiat. Meas*, vol. 59, pp. 262–269, Dec. 2013.

[103] K. Matsushita, T. Nishio, S. Tanaka, M. Tsuneda, A. Sugiura, and K. Ieki, "Measurement of proton induced target fragmentation cross sections in carbon," *Nucl. Phys. A*, vol. 946, pp. 104–116, Feb. 2016.

[104] A. Bongrand, E. Busato, P. Force, F. Martin, and G. Montarou, "Use of short-lived positron emitters for in-beam and real-time β^+ range monitoring in proton therapy," *Eur. J. Med. Phys.*, vol. 69, no. 1, pp. 248–255, 2020.

[105] A. Wrońska et al., "Prompt-gamma emission in GEANT4 revisited and confronted with experiment," *Eur. J. Med. Phys.*, vol. 88, no. 8, pp. 250–261, 2021.

[106] M. Pinto, D. Dauvergne, N. Freud, J. Krimmer, J. M. Létang, and E. Testa, "Assessment of GEANT4 prompt-gamma emission yields in the context of proton therapy monitoring," *Front. Oncol.*, vol. 6, no. 1, p. 10, 2016.

[107] J. Jeyasugiththan and S. Peterson, "Evaluation of proton inelastic reaction models in GEANT4 for prompt gamma production during proton radiotherapy," *Phys. Med. Biol.*, vol. 60, no. 9, pp. 7617–7635, 2015.

[108] G. Battistoni, M. Toppi, and V. Patera, "Measuring the impact of nuclear interaction in particle therapy and in radio protection in space: the FOOT experiment," *Front. Phys.*, vol. 8, Feb. 2021, Art. no. 568242.

[109] P. Kundrat et al., "Coupling radiation transport and track-structure simulations: Strategy based on analytical formulas representing DNA damage yields," *Front. Phys.*, vol. 9, Sep. 2021, Art. no. 719682.

[110] A. Rucinski, A. Biernacka, and R. Schulte, "Applications of nanodosimetry in particle therapy planning and beyond," *Phys. Med. Biol.*, vol. 66, no. 24, p. 10, 2021.

[111] S. Incerti, G. Baldacchino, and M. Bernal, "The GEANT4-DNA project," *Int. J. Model. Simulat. Sci. Comput.*, vol. 1, no. 2, pp. 157–178, 2010.

[112] J. Schuemann, A. McNamara, and J. Ramos-Méendez, "TOPAS-nBio: An extension to the TOPAS simulation toolkit for cellular and subcellular radiobiology," *Radiat. Res.*, vol. 191, no. 2, pp. 125–138, 2019.

[113] M. Scholz, A. Kellerer, W. Kraft-Weyrather, and G. Kraft, "Computation of cell survival in heavy ion beams for therapy—The model and its approximation," *Radiat. Environ. Biophys.*, vol. 36, no. 1, pp. 59–66, 1997.

[114] M. Krämer and M. Scholz, "Treatment planning for heavy-ion radiotherapy: Calculation and optimization of biologically effective dose," *Phys. Med. Biol*, vol. 45, no. 11, p. 3319, 2000.

[115] R. Hawkins, "A microdosimetric-kinetic model of cell death from exposure to ionizing radiation of any LET, with experimental and clinical applications," *Int. J. Radiat. Biol.*, vol. 69, no. 6, pp. 739–755, 1996.

[116] A. M. Kellerer and H. H. Rossi, "A generalized formulation of dual radiation action," *Radiat. Res.*, vol. 75, no. 3, pp. 471–88, 1978.

[117] Y. Kase et al., "Biological dose calculation with MC physics simulation for heavy-ion radiotherapy," *Phys. Med. Biol.*, vol. 51, no. 24, pp. N467–N475, 2006.

[118] G. Magro et al., "The FLUKA MC code coupled with the NIRS approach to clinical dose calculation in carbon ion therapy," *Phys. Med. Biol.*, vol. 62, no. 9, pp. 3814–3827, 2017.

[119] M. P. Carante, C. Aimè, J. J. T. Cajiao, and F. Ballarini, "BIANCA, a biophysical model of cell survival and chromosome damage by protons, C-ions and He-ions at energies and doses used in hadrontherapy," *Phys. Med. Biol.*, vol. 63, no. 7, 2018, Art. no. 75007.

[120] M. P. Carante, G. Aricò, A. Ferrari, W. Kozlowska, A. Mairani, and F. Ballarini, "First benchmarking of the BIANCA model for cell survival prediction in a clinical hadron therapy scenario," *Phys. Med. Biol.*, vol. 64, no. 21, 2019, Art. no. 215008.

[121] G. Russo et al., "A novel algorithm for the calculation of physical and biological irradiation quantities in scanned ion beam therapy: The beamlet superposition approach," *Phys. Med. Biol.*, vol. 61, no. 1, pp. 183–214, 2016.

[122] C. Grassberger, J. Daartz, S. Dowdell, T. Ruggieri, G. Sharp, and H. Paganetti, "Quantification of proton dose calculation accuracy in the lung," *Int. J. Radiat. Oncol. Biol. Phys.*, vol. 89, no. 2, pp. 424–430, 2014.

[123] A. Mairani et al., "A MC-based treatment planning tool for proton therapy," *Phys. Med. Biol.*, vol. 58, no. 8, p. 71, 2013.

[124] A. C. Kraan, N. Depauw, B. Clasie, M. Giunta, T. Madden, and H. M. Kooy, "Effects of spot parameters in pencil beam scanning treatment planning," *Med. Phys.*, vol. 45, no. 1, pp. 60–73, 2018.

[125] X. Jia, T. Pawlicki, K. Murphy, and A. Mundt, "Proton therapy dose calculations on GPU: advances and challenges," *Transl. Cancer Res.*, vol. 9, no. 4, p. 15, 2020.

[126] A. Schiavi et al., "FRED: A GPU-accelerated fast-MC code for rapid treatment plan recalculation in ion beam therapy," *Phys. Med. Biol.*, vol. 62, no. 18, pp. 7482–7504, 2017.

[127] D. Giantsoudi, J. Schuemann, X. Jia, S. Dowdell, S. Jiang, and H. Paganetti, "Validation of a GPU-based MC code (GPMC) for proton radiation therapy: Clinical cases study," *Phys. Med. Biol.*, vol. 60, no. 2, pp. 22570–2269, 2015.

[128] R. Kohno, K. Hotta, S. Nishioka, K. Matsubara, R. Tansho, and T. Suzuki, "Clinical implementation of a GPU-based simplified MC method for a treatment planning system of proton beam therapy," *Phys. Med. Biol.*, vol. 56, no. 11, pp. 287, 2011.

[129] H. Lee et al., "MOQUI: An open-source GPU-based MC code for proton dose calculation with efficient data structure," *Phys. Med. Biol.*, vol. 67, no. 8, p. 10, 2022.

[130] D. Maneval, H. Bouchard, B. Ozell, and P. Després, "Efficiency improvement in proton dose calculations with an equivalent restricted stopping power formalism," *Phys. Med. Biol.*, vol. 63, no. 10, 2017, Art. no. 15019.

[131] H. W. C. Tseung, J. Ma, and C. Beltran, "A fast GPU-based MC simulation of proton transport with detailed modeling of nonelastic interactions," *Med. Phys.*, vol. 42, no. 6, pp. 2967–2978, 2015.

[132] M. D. Pepin, E. Tryggestad, H. S. W. C. Tseung, J. E. Johnson, M. G. Herman, and C. Beltran, "A Monte-Carlo-based and GPU-accelerated 4D-dose calculator for a pencil beam scanning proton therapy system," *Med. Phys.*, vol. 45, no. 11, pp. 5293–5304, 2018.

[133] M. De Simoni et al., "A data-driven fragmentation model for carbon therapy GPU-accelerated Monte-Carlo dose recalculation," *Front. Oncol. Radiat. Oncol.*, vol. 12, Mar. 2022, Art. no. 780784. [Online]. Available: https://doi.org/10.3389/fonc.2022.780784

[134] N. Qin et al., "Initial development of GOCMC: A GPU-oriented fast cross-platform MC engine for carbon ion therapy," *Phys. Med. Biol.*, vol. 62, no. 1, pp. 3682–3699, May 2017.

[135] G. Kalantzis and H. Tachibana, "Accelerated event-by-event MC microdosimetric calculations of electron and proton tracks on a multi-core GPU and a CUDA-enabled GPU," *Comput. Methods Progr. Biomed.*, vol. 113, no. 1, pp. 116–125, 2014.

[136] S. Okada et al., "MPEXS-DNA, a new GPU-based MC simulator for track structures and radiation chemistry at subcellular scale," *Med. Phys.*, vol. 46, no. 3, pp. 1483–1500, May 2019.

[137] M.-Y. Tsai et al., "A new open-source GPU-based microscopic MC simulation tool for the calculations of DNA damages caused by ionizing radiation—Part I: Core algorithm and validation," *Med. Phys.*, vol. 47, no. 4, pp. 1958–1970, 2020.

[138] Q. Wang et al., "Automatic phase space generation for MC calculations of intensity modulated particle therapy," *Biomed. Phys. Eng. Exp.*, vol. 6, no. 2, 2020, Art. no. 25001.

[139] P. Lysakovski et al., "Development and benchmarking of a MC dose engine for proton radiation therapy," *Front. Phys.*, vol. 9, no. 11, 2021, Art. no. 741453.
[140] P. Lysakovski et al., "Development and validation of MonteRay, a fast Monte Carlo dose engine for carbon ion beam radiotherapy," *Med. Phys.*, vol. 51, no. 2, pp. 1433–1449, 2024.
[141] J. S. Li et al., "A particle track-repeating algorithm for proton beam dose calculation," *Phys. Med. Biol.*, vol. 50, no. 2, pp. 1001–1010, 2005.
[142] P. P. Yepes et al., "Validation of a track repeating algorithm for intensity modulated proton therapy: clinical cases study," *Phys. Med. Biol.*, vol. 61, no. 7, pp. 2633–2645, 2016.
[143] Q. Wang et al., "Validation of the fast dose calculator for Shanghai proton and heavy ion center," *Biomed. Phys. Eng. Exp.*, vol. 4, p. 6500, Sep. 2018.
[144] Q. Wang et al., "A track repeating algorithm for intensity modulated carbon ion therapy," *Phys. Med. Biol.*, vol. 64, no. 3, 2019, Art. no. 95026.
[145] M. Fippel and M. Soukup, "A MC dose calculation algorithm for proton therapy," *Med. Phys.*, vol. 31, no. 8, pp. 2263–2273, 2004.
[146] M. Fix, D. Frei, W. Volken, and E. Born, "Macro MC for dose calculation of proton beams," *Phys. Med. Biol.*, vol. 58, no. 7, pp. 2027–2044, 2013.
[147] J. Shan et al., "Virtual particle MC: A new concept to avoid simulating secondary particles in proton therapy dose calculation," *Med. Phys.*, vol. 49, no. 10, pp. 6666–6683, 2022.
[148] D. Maneval, H. Bouchard, B. Ozell, and P. Després, "Efficiency improvement in proton dose calculations with an equivalent restricted stopping power formalism," *Phys. Med. Biol.*, vol. 63, no. 1, 2018, Art. no. 015019.
[149] J. Saini et al., "Dosimetric evaluation of a commercial proton spot scanning Monte-Carlo dose algorithm: Comparisons against measurements and simulations," *Phys. Med. Biol.*, vol. 62, no. 19, pp. 7659–7681, 2017.
[150] F. Fracchiolla et al., "Clinical validation of a GPU-based MC dose engine of a commercial treatment planning system for pencil beam scanning proton therapy," *Eur. J. Med. Phys.*, vol. 88, pp. 226–234, Aug. 2021.
[151] L. Lin et al., "A benchmarking method to evaluate the accuracy of a commercial proton MC pencil beam scanning treatment planning system," *J. Appl. Clin. Med. Phys.*, vol. 18, no. 2, p. 44, 2017.
[152] L. Beaton, S. Bandula, M. Gaze, and R. Sharma, "How rapid advances in imaging are defining the future of precision radiation oncology," *Brit. J. Cancer*, vol. 120, no. 8, pp. 1–12, 2019.
[153] J. Unkelbach, T. Bortfeld, B. C. Martin, and M. Soukup, "Reducing the sensitivity of IMPT treatment plans to setup errors and range uncertainties via probabilistic treatment planning," *Med. Phys.*, vol. 36, no. 1, pp. 149–163, 2009.
[154] S. Stefanowicz, K. Stützer, S. Zschaeck, A. Jakobi, and E. G. C. Troost, "Comparison of different treatment planning approaches for intensity-modulated proton therapy with simultaneous integrated boost for pancreatic cancer," *Radiat. Oncol.*, vol. 13, no. 11, p. 228, 2018.
[155] W. Schneider, T. Bortfeld, and W. Schlegel, "Correlation between CT numbers and tissue parameters needed for MC simulations of clinical dose distributions," *Phys. Med. Biol.*, vol. 45, no. 2, pp. 459–478, 2000.
[156] M. Yang et al., "Comprehensive analysis of proton range uncertainties related to patient stopping-power-ratio estimation using the stoichiometric calibration," *Phys. Med. Biol.*, vol. 57, no. 6, pp. 4095–4115, 2012.
[157] W. V. Elmpt, G. Landry, M. Das, and F. Verhaegen, "Dual energy CT in radiotherapy: Current applications and future outlook," *Radiother. Oncol.*, vol. 119, no. 3, pp. 137–144, 2016.
[158] N. Peters et al., "Reduction of clinical safety margins in proton therapy enabled by the clinical implementation of dual-energy CT for direct stopping-power prediction," *Radiother. Oncol.*, vol. 166, no. 11, pp. 71–78, 2021.
[159] M. F. Spadea et al., "Deep convolution neural network (DCNN) multiplane approach to synthetic CT generation from MR images-application in brain proton therapy," *Int J. Radiat. Oncol. Biol. Phys.*, vol. 105, no. 3, pp. 495–503, Nov. 2019.
[160] G. Li, X. Wu, and X. Ma, "Artificial intelligence in radiotherapy," *Seminar Cancer Biol.*, vol. 86, no. 2, pp. 160–171, 2022.
[161] Y. Fu et al., "Artificial Intelligence in Radiation Therapy," *IEEE Trans. Radiat. Plasma Med. Sci.*, vol. 6, no. 2, pp. 158–181, May 2022.
[162] B. Gottschalk, "Techniques of proton radiotherapy: Transport theory," 2012, *arxiv.abs/1204.4470*.
[163] M. Rahman, P. Bruza, Y. Lin, D. J. Gladstone, B. W. Pogue, and R. Zhang, "Producing a beam model of the Varian probeam proton therapy system using TOPAS Monte Carlo toolkit," *Med. Phys.*, vol. 47, no. 12, pp. 6500–6508, 2020.
[164] L. Grevillot, D. Bertrand, F. Dessy, and D. Sarrut, "A MC pencil beam scanning model for proton treatment plan simulation using GATE/GEANT4," *Phys. Med. Biol.*, vol. 56, no. 8, pp. 5203–5219, 2011.
[165] T. Aso, K. Mastushita, T. Nishio, S. Kabuki, and T. Sasaki, "Extending Geant4 based particle therapy system simulation framework to medical imaging applications," in *Proc. IEEE Nucl. Sci. Symp. Med. Imag. Conf. (NSS/MIC)*, 2015, pp. 1–4.
[166] H. Fuchs et al., "Computer-assisted beam modeling for particle therapy," *Med. Phys.*, vol. 48, no. 2, pp. 841–851, 2021.
[167] J. Saini et al., "Advanced proton beam dosimetry—Part I: Review and performance evaluation of dose calculation algorithms," *Transl. Lung Cancer Res.*, vol. 7, no. 2, pp. 171–179, 2018.
[168] J. B. Farr et al., "Clinical commissioning of intensity-modulated proton therapy systems: Report of AAPM task group 185," *Med. Phys.*, vol. 48, no. 1, pp. e1–e30, 2021.
[169] L. Hong et al., "A pencil beam algorithm for proton dose calculations," *Phys. Med. Biol.*, vol. 41, no. 8, pp. 1305–1330, 1996.
[170] B. Schaffner, E. Pedroni, and A. Lomax, "Dose calculation models for proton treatment planning using a dynamic beam delivery system: an attempt to include density heterogeneity effects in the analytical dose calculation," *Phys. Med. Biol.*, vol. 44, no. 1, p. 27, 1999.
[171] D. Maes et al., "Validation and practical implementation of seated position radiotherapy in a commercial TPS for proton therapy," *Eur. J. Med. Phys.*, vol. 80, no. 12, pp. 175–185, 2020.
[172] P. Taylor, S. Kry, and D. Followill, "Pencil beam algorithms are unsuitable for proton dose calculations in lung," *Int. J. Radiat. Oncol. Biol. Phys.*, vol. 99, no. 6, pp. 750–756, 2017.
[173] B. Kopp et al., "FRoG: An independent dose and LET_d prediction tool for proton therapy at probeam facilities," *Med. Phys.*, vol. 47, no. 7, pp. 5274–5286, Oct. 2020.
[174] S. Mein et al., "Fast robust dose calculation on GPU for high-precision 1H, 4He, 12C and 16O ion therapy: the FRoG platform," *Sci. Rep.*, vol. 8, no. 1, 2018, Art. no. 14829.
[175] Y. Nomura et al., "Fast spot-scanning proton dose calculation method with uncertainty quantification using a three-dimensional convolutional neural network," *Phys. Med. Biol.*, vol. 65, p. 6, 2020, Art. no. 215007.
[176] C. Wu et al., "Improving proton dose calculation accuracy by using deep learning," *Mach. Learn. Sci. Technol.*, vol. 2, no. 1, p. 9, 2020.
[177] U. Oelfke and T. Bortfeld, "Inverse planning for photon and proton beams," *Med. Dosim.*, vol. 26, no. 2, pp. 113–124, 2001.
[178] Q. Wu and R. Mohan, "Algorithm and functionality of an intensity modulated radiotherapy optimization system," *Med. Phys.*, vol. 27, no. 5, pp. 701–711, 2000.
[179] K. L. Moore, "Automated radiotherapy treatment planning: Adaptive radiotherapy and automation," *Seminar Radiat. Oncol.*, vol. 29, no. 3, pp. 209–218, 2019.
[180] S. van de Water et al., "Improved efficiency of multi-criteria IMPT treatment planning using iterative resampling of randomly placed pencil beams," *Phys. Med. Biol.*, vol. 58, no. 9, pp. 6969–6983, 2013.
[181] Y. Li et al., "A new approach to integrate GPU-based MC simulation into inverse treatment plan optimization for proton therapy," *Phys. Med. Biol.*, vol. 62, no. 1, pp. 289–305, 2017.
[182] J. Ma, C. Beltran, H. S. W. C. Tseung, and M. G. Herman, "A GPU-accelerated and MC-based intensity modulated proton therapy optimization system," *Med. Phys.*, vol. 41, no. 12, 2014, Art. no. 121707.
[183] M. Durante, A. Golubev, W.-Y. Park, and C. Trautmann, "Applied nuclear physics at the new high-energy particle accelerator facilities," *Phys. Rep.*, vol. 800, no. 2, pp. 1–37, Apr. 2019, [Online]. Available: https://doi.org/10.1016/j.physrep.2019.01.004
[184] W. Cao et al., "Linear energy transfer incorporated intensity modulated proton therapy optimization," *Phys. Med. Biol.*, vol. 63, no. 11, 2017, Art. no. 15013.
[185] H.-P. Wieser et al., "matRAD—An open-source treatment planning toolkit for educational purposes," in *Proc. IFMBE*, vol. 51, 2018, p. 8.
[186] L. N. Burigo et al., "Simultaneous optimization of RBE-weighted dose and nanometric ionization distributions in treatment planning with carbon ions," *Phys. Med. Biol.*, vol.'64, no. 1, 2019, Art. no. 15015.
[187] M. Krämer, O. Jäkel, T. Haberer, G. Kraft, D. Schardt, and U. Weber, "Treatment planning for heavy-ion radiotherapy: physical

beam model and dose optimization," *Phys. Med. Biol.*, vol. 45, no. 1, pp. 3299–3317, 2000.

[188] O. Sokol et al., "Oxygen beams for therapy: Advanced biological treatment planning and experimental verification," *Phys. Med. Biol.*, vol. 62, no. 19, pp. 7798–7813, 2017.

[189] O. Sokol et al., "Kill painting of hypoxic tumors with multiple ion beams," *Phys. Med. Biol.*, vol. 64, no. 4, 2019, Art. no. 45008.

[190] M. Battestini, M. Schwarz, M. Krämer, and E. Scifoni, "Including volume effects in biological treatment plan optimization for carbon ion therapy: Generalized equivalent uniform dose-based objective in trip98," *Front. Oncol.*, vol. 12, no. 3, 2022, Art. no. 826414.

[191] T. Inaniwa, N. Kanematsu, K. Noda, and T. Kamada, "Treatment planning of intensity modulated composite particle therapy with dose and linear energy transfer optimization," *Phys. Med. Biol.*, vol. 62, no. 3, pp. 5180–5197, 2017.

[192] N. Qin et al., "Full MC-based biological treatment plan optimization system for intensity modulated carbon-ion therapy on GPU," *Int. J. Radiat. Biol. Phys.*, vol. 100, no. 1, pp. 235–243, 2018.

[193] H. Tseung et al., "Clinically applicable MC-based biological dose optimization for the treatment of head and neck cancers with spot-scanning proton therapy," *Int J. Radiat. Oncol. Biol. Phys.*, vol. 95, no. 4, pp. 1535–1543, 2016.

[194] H. Paganetti, "Range uncertainties in proton therapy and the role of MC simulations," *Phys. Med. Biol.*, vol. 57, no. 5, pp. 99–117, 2012.

[195] R. Mackay, "Image guidance for proton therapy," *Clin. Oncol.*, vol. 30, no. 3, pp. 293–298, 2018.

[196] L. Beaton, S. Bandula, M. Gaze, and R. Sharma, "How rapid advances in imaging are defining the future of precision radiation oncology," *Brit. J. Cancer*, vol. 120, no. 3, pp. 1–12, 2019.

[197] N. Hünemohr et al., "Experimental verification of ion stopping power prediction from dual energy CT data in tissue surrogates," *Phys. Med. Biol.*, vol. 59, no. 1, pp. 83–96, 2014.

[198] Y. Liu et al., "MRI-based treatment planning for proton radiotherapy: Dosimetric validation of a deep learning-based liver synthetic CT generation method," *Phys. Med. Biol.*, vol. 64, no. 5, 2019, Art. no. 145015.

[199] H. Chandarana, H. Wang, R. Tijssen, and I. Das, "Emerging role of MRI in radiation therapy," *J. Magn. Reson. Imag.*, vol. 48, no. 9, pp. 1468–1478, 2018.

[200] M. Unterrainer et al., "Recent advances of PET imaging in clinical radiation oncology," *Radiat. Oncol.*, vol. 15, no. 4, p. 88, 2020.

[201] M. Esposito et al., "Estimating dose delivery accuracy in stereotactic body radiation therapy: A review of in-vivo measurement methods," *Radiother. Oncol.*, vol. 149, no. 5, p. 319, 2020.

[202] S. Mashnik et al., "CEM03.03 and LAQGSM03.03 event generators for MCNP6, MCNPX and MARS15 transport codes," LANL, Los Alamos, NM, USA, Rep. LA-UR-08-2931, 2008.

[203] A. Ferrari and P. Sala, "The physics of high energy reactions," in *Proc. Workshop Nucl. Reaction Data Nucl. Reactor Phys. Design Safety ICTP*, vol. 2, 1998, pp. 424–532.

[204] A. Chatterjee, W. Saunders, E. L. Alpen, J. Alonso, J. Scherer, and J. Llacer, "Physical measurements with high-energy radioactive beams," *J. Radiat. Res.*, vol. 92, no. 2, pp. 230–244, 1982.

[205] K. Parodi and J. Polf, "*In Vivo* range verification in particle therapy," *Phys. Med*, vol. 45, no. 11, pp. e1036–e1050, 2018.

[206] A. D. Guerra et al., "A Monte Carlo simulation of the possible use of positron emission tomography in proton radiotherapy," *Nucl. Instrum. Methods Phys. Res. A, Accelerators, Spectrometers, Detectors Assoc. Equip.*, vol. 345, no. 2, pp. 379–384, 1994.

[207] A. Del Guerra, G. Di Domenico, and D. Mukhopadhayay, "PET dosimetry in proton radiotherapy: A mC study," *Appl. Radiat. Isot.*, vol. 48, no. 10, pp. 1617–1624, 1997.

[208] A. Knopf and A. Lomax, "*In-vivo* proton range verification: A review," *Phys. Med. Biol.*, vol. 58, no. 15, pp. 131–160, 2013.

[209] X. Zhu and G. E. Fahkri, "Proton therapy verification with PET imaging," *Theranostics*, vol. 3, no. 10, p. 731, 2013.

[210] K. Parodi, T. Yamaya, and P. Moskal, "Experience and new prospects of PET imaging for ion beam therapy monitoring," *Zeitschrift für Medizinische Physik*, vol. 33, no. 1, pp. 22–34, 2022.

[211] F. Attanasi et al., "Extension and validation of an analytical model for *in vivo* PET verification of proton therapy—A phantom and clinical study," *Phys. Med. Biol.*, vol. 56, no. 8, pp. 5079–5098, 2011.

[212] S. Ma et al., "Feasibility study of patient-specific dose verification in proton therapy utilizing positron emission tomography (PET) and generative adversarial network (GAN)," *Med. Phys.*, vol. 47, no. 8, pp. 5194–5208, 2020.

[213] A. Knopf et al., "Accuracy of proton beam range verification using post-treatment positron emission tomography/computed tomography as function of treatment site," *Int. J. Radiat. Oncol. Biol. Phys.*, vol. 79, no. 1, pp. 297–304, 2011.

[214] W. Enghardt et al., "Charged hadron tumour therapy monitoring by means of PET," *Nucl. Instrum. Methods Phys. Res. A, Accelerators, Spectrometers, Detectors Assoc. Equip.*, vol. 525, no. 1, pp. 284–288, 2004.

[215] T. Nishio et al., "Development and clinical use of beam on-line PET system mounted on a rotating gantry port in proton therapy," *Int. J. Radiat. Oncol. Biol. Phys.*, vol. 76, no. 1, pp. 277–286, 2010.

[216] V. Rosso et al., "DOPET: An in-treatment monitoring system for particle therapy," *Radiother. Oncol.*, vol. 118, no. 2, p. S92, 2016.

[217] G. Bisogni et al., "Inside in-beam positron emission tomography system for particle range monitoring in hadrontherapy," *J. Med. Imag.*, vol. 4, no. 12, 2016, Art. no. 11005.

[218] A. C. Kraan et al., "Localization of anatomical changes in patients during proton therapy with in-beam PET monitoring: A VBM approach exploiting MC simulations," *Med. Phys.*, vol. 49, no. 1, pp. 23–40, 2022.

[219] E. Fiorina et al., "Detection of interfractional morphological changes in proton therapy: A simulation and *in vivo* study with the inside in-beam PET," *Front. Phys.*, vol. 8, no. 1, 2021, Art. no. 578388.

[220] M. Moglioni et al., "*In-vivo* range verification analysis with in-beam PET data for patients treated with proton therapy at CNAO," *Front. Oncol.*, vol. 12, Sep. 2022, Art. no. 929949.

[221] P. Dendooven et al., "Short-lived positron emitters in beam-on PET imaging during proton therapy," *Phys. Med. Biol.*, vol. 60, no. 23, pp. 8923–8947, 2015.

[222] T. T. Böhlen et al., "Benchmarking nuclear models of FLUKA and GEANT4 for hadron therapy," *Phys. Med. Biol.*, vol. 55, no. 19, pp. 5833–5847, 2010.

[223] H. Tashima et al., "Development of a small single-ring OpenPET prototype with a novel transformable architecture," *Phys. Med. Biol.*, vol. 61, 2, pp. 1795–1809, 2016.

[224] G. Lovatti et al., "Design study of a novel geometrical arrangement for an in-beam small animal positron emission tomography scanner," *Phys. Med. Biol.*, vol. 68, no. 23, 2023, Art. no. 235005.

[225] K. W. Brzezinski et al., "Detection of range shifts in proton beam therapy using the J-PET scanner: A patient simulation study," *Phys. Med. Biol.*, vol. 68, Jun. 2023, Art. no. 145016.

[226] D. Boscolo et al., "Radioactive beams for image-guided particle therapy: The barb experiment at GSI," *Front. Oncol.*, vol. 11, no. 8, 2021, Art. no. 737050.

[227] D. Schaart, "Physics and technology of time-of-flight PET detectors," *Phys. Med. Biol.*, vol. 66, no. 3, p. 9, 2021.

[228] F. Stichelbaut and Y. Jongen, "Verification of the proton beams position in the patient by the detection of prompt gamma-rays emission," in *Proc. 39th Meeting PTCOG Group*, 2003, p. 5.

[229] C.-H. Min, C. H. Kim, M. Youn, and J.-W. Kim, "Prompt gamma measurements for locating the dose falloff region in the proton therapy," *Appl. Phys. Lett.*, vol. 89, no. 11, pp. 183–517, 2006.

[230] J. Krimmer, D. Dauvergne, J. Létang, and E. Testa, "Prompt-gamma monitoring in hadrontherapy: A review," *Nucl. Instrum. Methods Phys. Res. A, Accelerators, Spectrometers, Detectors Assoc. Equip.*, vol. 878, pp. 58–73, Jan. 2018.

[231] A. Wrońska, "Prompt gamma imaging in proton therapy—Status, challenges and developments," *J. Phys. Conf.*, vol. 1561, no. 1, 2020, Art. no. 12021.

[232] E. Testa et al., "Monitoring the Bragg peak location of 73-MeV/u carbon ions by means of prompt X-ray measurements," *Appl. Phys. Lett.*, vol. 93, no. 10, p. 85, 2008.

[233] C. Richter et al., "First clinical application of a prompt gamma based *in vivo* proton range verification system," *Radiother. Oncol.*, vol. 118, no. 1, pp. 232–237, 2016.

[234] Y. Xie et al., "Prompt gamma imaging for *in vivo* range verification of pencil beam scanning proton therapy," *Int. J. Radiat. Oncol. Biol. Phys.*, vol. 99, no. 5, pp. 210–218, 2017.

[235] J. Berthold et al., "First-in-human validation of CT-based proton range prediction using prompt gamma imaging in prostate cancer treatments," *Int. J. Radiat. Oncol. Biol. Phys.*, vol. 111, no. 4, pp. 1033–1043, 2021.

[236] J. Park et al., "Multi-slit prompt-gamma camera for locating of distal dose falloff in proton therapy," *Nucl. Eng. Technol.*, vol. 51, no. 3, pp. 1406–1416, Aug. 2019.

[237] J.-W. Kim, "Pinhole camera measurements of prompt gamma-rays for detection of beam range variation in proton therapy," *J. Korean Phys. Soc.*, vol. 55, no. 10, pp. 1673–1676, 2009.

[238] J. C Polf, S. Avery, D. S. Mackin, and S. Beddar, "Imaging of prompt gamma rays emitted during delivery of clinical proton beams with a Compton camera: feasibility studies for range verification," *Phys. Med. Biol.*, vol. 60, no. 18, pp. 7085–7099, 2015.
[239] E. Muñoz et al., "Proton range verification with MACACO II Compton camera enhanced by a neural network for event selection," *Sci. Rep.*, vol. 11, p. 9325, Apr. 2021.
[240] J. Verburg and J. Seco, "Proton range verification through prompt gamma-ray spectroscopy," *Phys. Med. Biol.*, vol. 59, no. 11, pp. 7089–7106, 2014.
[241] F. Hueso-González, M. Rabe, T. A. Ruggieri, T. Bortfeld, and J. M. Verburg, "A full-scale clinical prototype for proton range verification using prompt gamma-ray spectroscopy," *Phys. Med. Biol.*, vol. 63, no. 7, 2018, Art. no. 185019.
[242] P. M. Martins, H. Freitas, T. Tessonnier, B. Ackermann, S. Brons, and J. Seco, "Towards real-time PGS range monitoring in proton therapy of prostate cancer," *Sci. Rep.*, vol. 11, no. 1, 2021, Art. no. 15331.
[243] C. Golnik et al., "Range assessment in particle therapy based on prompt-gamma-ray timing measurements," *Phys. Med. Biol.*, vol. 59, no. 8, 2014, Art. no. 5399.
[244] M. Testa, C. H. Min, J. M. Verburg, J. Schümann, H.-M. Lu, and H. Paganetti, "Range verification of passively scattered proton beams based on prompt gamma time patterns," *Phys. Med. Biol.*, vol. 59, no. 7, pp. 4181–4195, 2014.
[245] M. Jacquet et al., "A time-of-flight-based reconstruction for real-time prompt-gamma imaging in proton therapy," *Phys. Med. Biol.*, vol. 66, no. 13, 2021, Art. no. 135003.
[246] M. Jacquet et al., "A high sensitivity Cherenkov detector for prompt gamma timing and time imaging," *Sci. Rep.*, vol. 13, p. 3609, Mar. 2023.
[247] V. Ferrero et al., "Estimating the stopping power distribution during proton therapy: A proof of concept," *Front. Phys.*, vol. 10, no. 9, 2022, Art. no. 971767.
[248] F. Pennazio et al., "Proton therapy monitoring: spatiotemporal emission reconstruction with prompt gamma timing and implementation with PET detectors," *Phys. Med. Biol.*, vol. 67, no. 6, 2022, Art. no. 65005.
[249] Y. Chi, A. Chalise, Y. Shao, and M. Jin, "Comparison of prompt gamma yield from C-11 and C-12 ion beams using MC simulation," in *Proc. IEEE Nucl. Sci. Symp. Med. Imag. Conf. (NSS/MIC)*, 2018, pp. 1–3.
[250] G. Cartechini et al., "Loading the tumor with 31P, 63Cu and 89Y provides an in vivo prompt gamma-based range verification for therapeutic protons," *Front. Phys.*, vol. 11, p. 5, Feb. 2023.
[251] U. Amaldi et al., "Advanced quality assurance for CNAO," *Nucl. Instrum. Methods Phys. Res. A, Accelerators, Spectrometers, Detectors Assoc. Equip.*, vol. 617, nos. 1–3, p. 248, 2010.
[252] P. Henriquet et al., "Interaction vertex imaging (IVI) for carbon ion therapy monitoring: A feasibility study," *Phys. Med. Biol.*, vol. 57, no. 7, pp. 4655–4669, 2012.
[253] K. Gwosch et al., "Non-invasive monotoring of therapeutic carbon-ion beams in a homogeneous phantom by tracking of secondary ions," *Phys. Med. Biol.*, vol. 58, no. 11, 2013, Art. no. 3755.
[254] A. Rucinski et al., "Secondary radiation measurements for particle therapy applications: Charged particles produced by 4He and 12C ion beams in a PMMA target at large angle," *Phys. Med. Biol.*, vol. 63, no. 5, 2018, Art. no. 55018.
[255] M. Fischetti et al., "Inter-fractional monitoring of 12C ions treatments: Results from a clinical trial at the CNAO facility," *Sci. Rep.*, vol. 10, no. 11, 2020, Art. no. 20735.
[256] G. Traini et al., "Review and performance of the dose profiler, a particle therapy treatments online monitor," *Eur. J. Med. Phys.*, vol. 65, no. 9, pp. 84–93, 2019.
[257] R. Hälg and U. Schneider, "Neutron dose and its measurement in proton therapy—Current state of knowledge," *Brit. J. Radiol.*, vol. 93, no. 12, 2019, Art. no. 20190412.
[258] S. Clarke et al., "A scintillator-based approach to monitor secondary neutron production during proton therapy," *Med. Phys.*, vol. 43, no. 11, pp. 5915–5924, 2016.
[259] M. Toppi et al., "The MONDO tracker: Characterisation and study of secondary ultrafast neutrons production in carbon ion radiotherapy," *Front. Phys. Security Radiat. Detect.*, vol. 8, p. 12, Nov. 2020.
[260] K. Ytre-Hauge, K. Skjerdal, J. Mattingly, and I. Meric, "A MC feasibility study for neutron based real-time range verification in proton therapy," *Sci. Rep.*, vol. 9, no. 2, p. 2011, 2019.
[261] D. F. DeJongh et al., "A comparison of proton stopping power measured with proton CT and X-ray CT in fresh postmortem porcine structures," *Med. Phys.*, vol. 48, no. 12, pp. 7998–8009, 2021.
[262] R. Johnson et al., "Review of medical radiography and tomography with proton beams," *Rep. Progr. Phys.*, vol. 81, no. 9, 2017, Art. no. 16701.
[263] G. Poludniowski, N. Allinson, and P. Evans, "Proton radiography and tomography with application to proton therapy," *Brit. J. Radiol.*, vol. 88, no. 6, 2015, Art. no. 20150134.
[264] A. Cormack, "Representation of a function by its line integrals, with some radiological applications," *J. Appl. Phys.*, vol. 34, pp. 2722–2727, Sep. 1963.
[265] R. Schulte et al., "Conceptual design of a proton computed tomography system for applications in proton radiation therapy," *IEEE Trans. Nucl. Sci.*, vol. 51, no. 7, pp. 866–872, Jun. 2004.
[266] R. P. Johnson et al., "A fast experimental scanner for proton CT: Technical performance and first experience with phantom scans," *IEEE Trans. Nucl. Sci.*, vol. 63, no. 1, pp. 52–60, Feb. 2016.
[267] T. Gehrke, R. Gallas, O. Jäkel, and M. Martišíková, "Proof of principle of helium-beam radiography using silicon pixel detectors for energy deposition measurement, identification, and tracking of single ions," *Med. Phys.*, vol. 45, no. 12, pp. 817–829, 2017.
[268] I. Rinaldi, S. Brons, O. Jäkel, B. Voss, and K. Parodi, "Experimental investigations on carbon ion scanning radiography using a range telescope," *Phys. Med. Biol.*, vol. 59, no. 12, 2014, Art. no. 3041.
[269] L. Magallanes et al., "Upgrading an integrating carbon-ion transmission imaging system with active scanning beam delivery toward low dose ion imaging," *IEEE Trans. Radiat. Plasma Med. Sci.*, vol. 4, no. 2, pp. 262–268, Mar. 2020.
[270] D. Mazzucconi et al., "Mixed particle beam for simultaneous treatment and online range verification in carbon ion therapy: Proof-of-concept study," *Med. Phys.*, vol. 45, no. 11, pp. 5234–5243, 2018.
[271] L. Volz et al., "Experimental exploration of a mixed helium/carbon beam for online treatment monitoring in carbon ion beam therapy," *Phys. Med. Biol.*, vol. 65, no. 5, 2020, Art. no. 55002.
[272] R. Simpson et al., "Scaling of laser-driven electron and proton acceleration as a function of laser pulse duration, energy, and intensity in the multi-picosecond regime," *Phys. Plasmas*, vol. 28, no. 1, 2021, Art. no. 13108.
[273] G. Caporaso, Y.-J. Chen, and S. Sampayan, "The dielectric wall accelerator," *Rev. Accelerator Sci. Technol.*, vol. 2, no. 12, p. 12, 2009.
[274] X. Li et al., "The first prototype of spot-scanning proton arc treatment delivery," *Radiother. Oncol.*, vol. 137, pp. 130–136, Aug. 2019.
[275] B. A. de Jong et al., "Spot scanning proton arc therapy reduces toxicity in oropharyngeal cancer patients," *Med. Phys.*, vol. 50, no. 3, pp. 1305–1317, 2021.
[276] S. Mein et al., "Biological dose optimization for particle arc therapy using helium and carbon ions," *Int. J. Radiat. Oncol. Biol. Phys.*, vol. 114, no. 4, pp. 334–348, 2022.
[277] J. Unkelbach et al., "Joint optimization of radiotherapy treatments involving multiple radiation modalities," *IEEE Trans. Radiat. Plasma Med. Sci.*, vol. 6, no. 3, pp. 294–303, Mar. 2022.
[278] V. Favaudon et al., "Ultrahigh dose-rate flash irradiation increases the differential response between normal and tumor tissue in mice," *Sci. Transl. Med.*, vol. 6, no. 7, 2014, Art. no. 245ra93.
[279] Y. Prezado and G. R. Fois, "Proton-minibeam radiation therapy: A proof of concept," *Med. Phys.*, vol. 40, no. 3, 2013, Art. no. 31712.
[280] R. Barth, A. Soloway, and R. Fairchild, "Boron neutron capture therapy of cancer," *Cancer Res.*, vol. 50, no. 12, p. 1061, 1990.
[281] I. Meric et al., "A hybrid multi-particle approach to range assessment-based treatment verification in particle therapy," *Sci. Rep.*, vol. 13, p. 6709, Apr. 2023.
[282] W. Assmann et al., "Iono-acoustic characterization of the proton Bragg peak with submillimeter accuracy," *J. Med. Phys.*, vol. 42, no. 2, pp. 567–574, 2015.
[283] J. Schauer et al., "Range verification of a clinical proton beam in an abdominal phantom by co-registration of ionoacoustics and ultrasound," *Phys. Med. Biol.*, vol. 68, no. 12, 2023, Art. no. 125009.
[284] Z. Jiang et al., "3-D in-vivo dose verification in prostate proton therapy with deep learning-based proton-acoustic imaging," *Phys. Med. Biol.*, vol. 67, no. 21, 2022, Art. no. 215012.